Toward complete spectroscopy of ^{128}Pr and rotational structures in ^{126}Pr

D. J. Hartley, L. L. Riedinger, M. Danchev,* W. Reviol,† O. Zeidan, and Jing-ye Zhang
Department of Physics and Astronomy, University of Tennessee, Knoxville, Tennessee 37996

A. Galindo-Uribarri, C. J. Gross,‡ C. Baktash, M. Lipoglavsek,§ S. D. Paul,‖ D. C. Radford, and C.-H. Yu
Physics Division, Oak Ridge National Laboratory, Oak Ridge, Tennessee 37831

D. G. Sarantites and M. Devlin¶
Chemistry Department, Washington University, St. Louis, Missouri 63130

M. P. Carpenter, R. V. F. Janssens, and D. Seweryniak
Physics Division, Argonne National Laboratory, Argonne, Illinois 60439

E. Padilla
Instituto de Ciencias Nucleares, UNAM, 04510 Mexico, Distrito Federal, Mexico
(Received 4 December 2001; published 5 April 2002)

Over 240 transitions and three new rotational bands have been observed in the well-deformed, odd-odd $^{128}_{59}Pr_{69}$ nucleus. The high-spin states were populated in two experiments using the ^{92}Mo(^{40}Ca,3pn) reaction at beam energies of 170 and 184 MeV. Several structures were confirmed in the former experiment using the Clarion and HyBall arrays with the recoil mass spectrometer at Oak Ridge National Laboratory. Gammasphere, in conjunction with the Microball, were employed in the latter experiment at Argonne National Laboratory to extend the sequences to very high spins. Rotational structures in ^{126}Pr were also identified in the αpn channel of the same reaction. The recent discrepancies of spin assignments for the yrast bands in ^{126,128}Pr and the interpretation of the lowest crossing in the $\pi h_{11/2}$ band in ^{127}Pr are discussed. An adiabatic crossing of the intruder $i_{13/2}$ neutron with one of the normal-deformed bands in ^{128}Pr is observed at high rotational frequency. Experimental trends in the signature inversion phenomenon of the $\pi h_{11/2}\nu h_{11/2}$ bands in the $A\approx 130$ region are defined and prove to be surprisingly irregular with respect to those found in the $\pi h_{11/2}\nu i_{13/2}$ bands of the $A\approx 160$ region.

DOI: 10.1103/PhysRevC.65.044329 PACS number(s): 21.10.Re, 23.20.Lv, 27.60.+j

I. INTRODUCTION

Historically, odd-odd nuclei have not received nearly as much attention as their even-even and odd-A siblings. This is primarily due to the complexity and high density of low-energy states resulting from various couplings of valence protons and neutrons. While heavy-ion fusion reactions allow for the population of rotational bands well above this sea of states, positively identifying these structures with a particular odd-odd nucleus can be quite difficult as they may be based on low-energy isomers, and therefore are not seen in prompt coincidence with known transitions. However, with the advent of modern-day arrays, detailed studies of odd-odd nuclei with $150<A<180$ have produced comprehensive level schemes and valuable spectroscopic information exclusively obtainable from these complex nuclear systems (see, for example, Refs. [1–4]).

In the neutron-deficient mass 130 region, studies of odd-odd nuclei have proven to be fertile ground for nuclear structure phenomena such as signature inversion [5], prolate-oblate shape competition [6], highly deformed bands (see Ref. [7] and references therein), and most recently the possibility of chiral-twin bands [8]. However, little was known in the nuclei approaching the proton drip line, as a sundry of nuclei ($>$15) can be populated in the same experiment from multiple charged-particle emission channels of the proton-rich compound nucleus. This made spectroscopic studies difficult as γ rays from more than 15 different residual nuclei are present. The development of light charged-particle (protons and alphas) detector arrays with nearly 4π coverage, such as Microball [9] and HyBall [10,11], in combination with large Ge detector arrays, allows for the selection of γ rays in coincidence with a certain charged-particle channel. Thus, detailed spectroscopy is now possible in these nuclei that are far from stability.

Recently we reported the first evidence of excited states in the odd-odd nucleus $^{126}_{59}Pr_{67}$ [12], which is only two neutrons from the predicted proton drip line [13]. From these same experiments, we were able to positively identify three new

*Permanent address: Faculty of Physics, St. Kliment Ohridsky University of Sofia, BG-1164 Sofia, Bulgaria.
†Present address: Chemistry Department, Washington University, St. Louis, MO 63130.
‡Also at Oak Ridge Institute of Science and Education, Oak Ridge, TN 37831.
§Present address: J. Stefan Institute, Ljubljana, Slovenia.
‖Present address: Department of Nuclear and Atomic Physics, Tata Institute of Fundamental Research, Mumbai 400 005, India.
¶Present address: Los Alamos National Laboratory, Los Alamos, NM 87545.

rotational bands in ^{128}Pr. Over 140 new transitions were placed into one of the most extensive levels schemes in the region as it contains more than 240 transitions. In this paper, we describe the ^{128}Pr structures and provide a full discussion on the ^{126}Pr bands. We have confirmed and extended the possible highly deformed $\pi g_{9/2}\nu h_{11/2}$ band [14], along with observing the influence of the deformation-driving $i_{13/2}$ neutron at the highest frequencies. A systematic study of the signature inversion phenomenon has been performed for the $\pi h_{11/2}\nu h_{11/2}$ bands in the $A\approx 130$ region.

II. EXPERIMENTAL DETAILS

Two experiments were performed using the ^{92}Mo(^{40}Ca,αpn) and ^{92}Mo(^{40}Ca,$3pn$) reactions to populate high-spin states in ^{126}Pr and ^{128}Pr, respectively. In one experiment, a thin ($\sim 450 \mu$g/cm^2) self-supporting ^{92}Mo target was bombarded by a 170-MeV ^{40}Ca beam, provided by the 25-MV tandem accelerator of the Holifield Radioactive Ion Beam Facility at Oak Ridge National Laboratory (ORNL). A combination of the Clarion Ge array, the HyBall CsI array, and the recoil mass spectrometer (RMS) [11] was utilized to correlate the emitted γ rays, evaporated charged particles, and recoil mass on an event-by-event basis. γ rays were detected with the Clarion array, which consists of 11 clover Ge detectors, and was complemented with ten smaller single-crystal Ge detectors. HyBall is an array of 95 CsI scintillators coupled to photodiodes in a 4π configuration for the detection of light charged particles emitted by the compound nuclei. Reaction products recoiling from the target were separated by the RMS at the focal plane according to their mass-to-charge ratio A/Q. The RMS has acceptances of $\pm 10\%$ in recoil ion energy and $\pm 5\%$ in mass-to-charge ratio. A multiwired, gas-filled position-sensitive avalanche counter (PSAC) was used to detect the spatial distribution of the mass groups at the focal plane. The RMS was tuned for central recoils of mass $A=129$, energy $E=40.4$ MeV, and charge state $Q=20.5^+$. A charge-reset foil was placed ~ 10 cm behind the target in order to improve [15] the detection efficiency of recoils with highly converted transitions near the ground state. Observation of the ^{128}Pr recoils improved by a factor of 2–3 with the reset foil. The trigger conditions consisted of either two Ge signals in coincidence with a PSAC signal (γ-γ recoil) or four Ge signals with a HyBall event. γ rays associated with masses 126 and 128 were sorted into separate $E_\gamma \times E_\gamma$ matrices, as well as E_γ vs charged particle matrices. A total of $\sim 0.9\times 10^6$ and $\sim 4.5 \times 10^6$ γ-γ events were observed in the 126 and 128 mass-gated matrices, respectively. The data were analyzed with the RADWARE [16] suite of programs.

Combining the power of the Gammasphere spectrometer [17] with the selectivity of the Microball [9], we performed a second experiment with an emphasis on populating the highest spin states possible. The ^{40}Ca beam was accelerated to an energy of 184 MeV by the ATLAS facility at Argonne National Laboratory (ANL). Gammasphere consisted of 99 suppressed Ge detectors and collected $\sim 580\times 10^6$ fivefold or higher prompt γ-ray coincidence events. Events that were associated with the emission of αp and $3p$ were sorted into separate $E_\gamma \times E_\gamma \times E_\gamma$ cubes, which made up $\sim 7.5\%$ and 13% of the total number of events recorded, respectively. The RADWARE package was also used in the analysis of these data.

Directional correlation of oriented states (DCO) [18] analysis was performed with the Gammasphere data in order to determine the relative spin of the states. Asymmetric matrices were created where γ-ray energies observed in the detectors near 35° and 145° were histogrammed along one axis and coincident γ rays found in detectors near 90° were histogrammed along the other axis. With a gate on an $E2(\Delta I = 2)$ transition(s), DCO ratios of 0.5 and 1.0 are expected for pure dipole ($M1$ and $E1$) and quadrupole ($E2$) transitions, respectively. Tables I and II contain the measured DCO ratios along with energy, spin, and parity of the states, as well as the energy and relative intensity of the depopulating γ rays for ^{128}Pr and ^{126}Pr, respectively.

The relative cross sections of the $\alpha 2p$(^{126}Ce),$4p$(^{128}Ce), and $4pn$(^{127}Ce) channels, with respect to the strongest $3p$(^{129}Pr) channel, were determined from the total projection of the ORNL experiment. Although the trigger conditions employed for the experiment make absolute measurements of the relative yields difficult, one may still extract a reasonable estimate for the production of these nuclei. Relative cross sections of other $A=126$, 127, 128, and 129 recoils were determined from mass-gated total projections and were normalized with respect to the channels specifically noted above. The results are displayed in Table III, where the experimental values are compared with the calculated relative cross sections from HIVAP using a beam energy of 170 MeV and standard parameters [19]. A good agreement is generally seen for all the channels except for the underestimation of the $\alpha 2p$ channel. We have also provided in Table III the absolute cross sections calculated by HIVAP in order to give an approximation of σ for each of the channels measured.

A. The ^{128}Pr level scheme

Previously, four structures have been associated with ^{128}Pr. Watson *et al.* [20] identified a strongly coupled band, which was confirmed in a recent publication with the present data [12], as well as two other coupled sequences. Smith *et al.* [14] reported a possibly highly deformed sequence from an experiment utilizing Gammasphere and the Microball. From the present work, these four structures were extended to higher spins and three new bands have been observed for the first time. Due to the extensive nature of the level scheme, it has been divided into two parts, with proposed positive-parity bands shown in Fig. 1 and the negative-parity bands shown in Fig. 3. Unfortunately, no connecting transitions between the positive- and negative-parity states were observed. As is common with most odd-odd nuclei, the high-spin structures could not be definitively linked to the ground state, which is suggested to have $I^\pi = (3^+)$ [21]; therefore, spin and parity assignments must be considered tentative.

1. Positive-parity bands in ^{128}Pr

Watson *et al.* [20], using a mass separator with an array of Ge detectors, observed the structure labeled as band 1 in Fig.

TABLE I. Data for levels and γ rays in ^{128}Pr.

I_i^{π} [a]	E_{level} (keV)	E_γ (keV)[b]	I_γ[c]	DCO	Multipolarity	Band$_f$[d]
		Band 1: $\pi h_{11/2}\nu h_{11/2}$, α=0				
(8^+)	X+93.5	93.5	[e]	0.60(8)	$M1/E2$	1
(10^+)	X+384.4	291.0	26(1)	1.03(6)	$E2$	1
		156.8	97(4)	0.47(2)	$M1/E2$	1
(12^+)	X+816.0	431.6	53(2)	0.96(3)	$E2$	1
		220.4	66(3)	0.47(2)	$M1/E2$	1
(14^+)	X+1381.6	565.6	59(3)	1.00(4)	$E2$	1
		283.1	39(3)	0.38(2) [f]	$M1/E2$	1
(16^+)	X+2062.7	681.1	44(2)	0.99(4)	$E2$	1
		342.1	20.9(9)	0.47(6)	$M1/E2$	1
(18^+)	X+2835.8	773.1	30(1)	0.98(4)	$E2$	1
		395.0	11.9(6)	0.37(6)	$M1/E2$	1
(20^+)	X+3683.2	847.4	22(1)	0.94(5)	$E2$	1
		444.6	6.0(4)	0.51(6)	$M1/E2$	1
(22^+)	X+4602.8	919.6	14.0(7)	0.96(7)	$E2$	1
		498.1	5.4(3)		($M1/E2$)	1
(24^+)	X+5606.5	1003.7	10.1(5)	1.1(1)	$E2$	1
		559.9	2.3(5)		($M1/E2$)	1
(26^+)	X+6707.4	1100.9	5.0(3)	1.0(1)	$E2$	1
(28^+)	X+7912.4	1205.0	2.5(2)		($E2$)	1
(30^+)	X+9224.3	1311.9	$<$2		($E2$)	1
(32^+)	X+10641.9	1417.6	$<$2		($E2$)	1
(34^+)	X+(12144)	(1502)	$<$2		($E2$)	1
		Band 1: $\pi h_{11/2}\nu h_{11/2}$, α=1				
(7^+)	X					
(9^+)	X+227.6	227.6	14.4(7)		($E2$)	1
		134.1	$\equiv$100	0.49(2)	$M1/E2$	1
(11^+)	X+595.5	368.1	32(2)	0.99(5)	$E2$	1
		211.1	83(4)	0.47(2)	$M1/E2$	1
(13^+)	X+1098.4	502.9	39(2)	1.04(7)	$E2$	1
		282.4	45(3)	0.38(2)[f]	$M1/E2$	1
(15^+)	X+1720.2	621.8	39(2)	1.00(5)	$E2$	1
		338.7	28(1)	0.40(5)	$M1/E2$	1
(17^+)	X+2440.5	720.3	36(2)	1.01(5)	$E2$	1
		377.9	18.7(9)	0.37(5)	$M1/E2$	1
(19^+)	X+3238.0	797.5	27(1)	0.97(9)	$E2$	1
		402.7	10.4(5)	0.41(6)	$M1/E2$	1
(21^+)	X+4104.6	866.6	21(1)	0.84(9)	$E2$	1
		421.8	6.5(3)	0.43(8)	$M1/E2$	1
(23^+)	X+5046.4	941.8	13.9(7)	1.0(1)	$E2$	1
		444.0	3.8(3)	0.51(6)	$M1/E2$	1
(25^+)	X+6074.4	1028.0	9.9(5)	1.0(1)	$E2$	1
		468.2	$<$2		($M1/E2$)	1
(27^+)	X+7193.5	1119.1	5.7(3)		($E2$)	1
(29^+)	X+8405.4	1211.9	3.4(2)		($E2$)	1
(31^+)	X+9708.3	1302.9	$<$2		($E2$)	1
(33^+)	X+11099.9	1391.6	$<$2		($E2$)	1
(35^+)	X+12585.1	1485.2	$<$2		($E2$)	1
(37^+)	X+14157.5	1572.4	$<$2		($E2$)	1

TABLE I. *(Continued.)*

I_i^{π} [a]	E_{level} (keV)	E_γ (keV)[b]	I_γ[c]	DCO	Multipolarity	Band$_f$[d]
		Band 2: $\pi h_{11/2}\nu h_{9/2}$, $\alpha=1$				
(7^+)	$X+470.9$	333.1	[e]			
(9^+)	$X+741.2$	270.3	<2		$(E2)$	2
		356.8	<2	0.6(1)	$M1/E2$	1
(11^+)	$X+1126.4$	385.2	4.1(3)	1.07(8)	$E2$	2
		346.9	2.1(2)	0.7(1)	$M1/E2$	3
(13^+)	$X+1610.8$	484.4	4.2(3)	0.92(7)	$E2$	2
		573.8	4.3(3)	0.9(1)	$E2$	3
		290.2	<2		$(M1/E2)$	3
(15^+)	$X+2229.7$	618.9	8.3(5)	0.99(5)	$E2$	2
(17^+)	$X+2942.9$	713.2	8.1(5)	1.07(6)	$E2$	2
(19^+)	$X+3742.6$	799.7	6.7(4)	1.04(5)	$E2$	2
(21^+)	$X+4621.5$	878.9	6.0(3)	0.95(6)	$E2$	2
(23^+)	$X+5580.7$	959.2	3.7(2)	1.2(1)	$E2$	2
(25^+)	$X+6624.6$	1043.9	2.5(2)	0.9(1)	$E2$	2
(27^+)	$X+7748.5$	1123.9	2.1(2)		$(E2)$	2
(29^+)	$X+8931.2$	1182.7	<2		$(E2)$	2
(31^+)	$X+10163.2$	1232.0	<2		$(E2)$	2
(33^+)	$X+11457.7$	1294.5	<2		$(E2)$	2
(35^+)	$X+12825.9$	1368.2	<2		$(E2)$	2
(37^+)	$X+14273.6$	1447.7	<2		$(E2)$	2
(39^+)	$X+(15791)$	(1517)	<2		$(E2)$	2
		Band 3: $\alpha=0$				
(10^+)	$X+779.2$	210.9	3.1(4)		$(M1/E2)$	3
(12^+)	$X+1320.4$	(541)	<2		$(E2)$	3
		283	<2		$(M1/E2)$	3
(14^+)	$X+1989$	669	<2		$(E2)$	3
		Band 3: $\alpha=1$				
(9^+)	$X+568.6$	183.5	<2		$(M1/E2)$	1
(11^+)	$X+1037.0$	468.4	<2		$(E2)$	3
		257.2	3.4(2)		$(M1/E2)$	3
		220.6	2.6(4)		$(M1/E2)$	1
(13^+)	$X+1665$	628	2.5(3)		$(E2)$	3
		345	<2		$(M1/E2)$	3
		Band 4: $\alpha=0$				
(14^+)	$X+2123.2$	264.3	3.7(2)		$(M1/E2)$	4
		536.2	3.3(3)			
		741.6	<2		$(E2)$	1
		1024.7	<2		$(M1/E2)$	1
(16^+)	$X+2773.8$	650.6	4.3(4)		$(E2)$	4
		324.5	3.9(6)		$(M1/E2)$	4
(18^+)	$X+3523.3$	749.5	3.8(4)		$(E2)$	4
		378.6	4.3(3)		$(M1/E2)$	4
(20^+)	$X+4353.0$	829.7	4.0(4)		$(E2)$	4
		420.8	3.0(2)		$(M1/E2)$	4
(22^+)	$X+5252.8$	899.8	5.0(3)		$(E2)$	4
		458.4	2.9(2)		$(M1/E2)$	4
(24^+)	$X+6231.0$	978.2	3.2(3)		$(E2)$	4
		501.5	<2		$(M1/E2)$	4
(26^+)	$X+7298.9$	1067.9	<2		$(E2)$	4
		548.2	<2		$(M1/E2)$	4
(28^+)	$X+8464.2$	1165.3	<2		$(E2)$	4
(30^+)	$X+9727$	1263	<2		$(E2)$	4

TABLE I. *(Continued.)*

I_i^{π} [a]	E_{level} (keV)	E_γ (keV)[b]	I_γ[c]	DCO	Multipolarity	Band$_f$[d]
		Band 4: $\alpha=1$				
(13^+)	$X+1858.9$	(1044)	<2		$(M1/E2)$	1
(15^+)	$X+2450.1$	591.2	3.6(4)		$(E2)$	4
		326.5	5.1(8)		$(M1/E2)$	4
(17^+)	$X+3146.1$	696.0	4.9(4)		$(E2)$	4
		371.4	4.9(4)		$(M1/E2)$	4
(19^+)	$X+3933.3$	787.2	3.8(3)		$(E2)$	4
		408.3	2.5(2)		$(M1/E2)$	4
(21^+)	$X+4795.6$	862.3	3.6(3)		$(E2)$	4
		441.2	2.9(2)		$(M1/E2)$	4
(23^+)	$X+5731.5$	935.9	3.8(3)		$(E2)$	4
		477.5	<2		$(M1/E2)$	4
(25^+)	$X+6752.0$	1020.5	2.0(2)		$(E2)$	4
		519.1	<2		$(M1/E2)$	4
(27^+)	$X+7866.5$	1114.5	<2		$(E2)$	4
(29^+)	$X+9079.1$	1212.6	<2		$(E2)$	4
(31^+)	$X+10386$	1307	<2		$(E2)$	4
		Band 5: $\pi h_{11/2}\nu(d_{3/2}/s_{1/2})$, $\alpha=0$				
(6^-)	$Y+151.8$					
(8^-)	$Y+387.9$	236.1	3.5(4)		$(E2)$	5
		147.0	19(1)	0.6(1)	$M1/E2$	5
		271.5	7.0(6)	0.6(1)		
(10^-)	$Y+788.3$	400.4	15(1)	1.00(9)	$E2$	5
		243.0	8.2(6)	0.8(1)	$M1/E2$	5
		226.3	3.1(3)	0.8(1)	$M1/E2$	6
(12^-)	$Y+1317.8$	529.5	17.7(9)	1.00(9)	$E2$	5
		332.5	2.1(2)		$(M1/E2)$	5
		303.0	4.1(3)		$(M1/E2)$	6
(14^-)	$Y+1954.7$	636.9	16.5(8)	1.0(1)	$E2$	5
		355.6	3.7(3)		$(M1/E2)$	6
(16^-)	$Y+2676.6$	721.9	10.8(7)	1.1(1)	$E2$	5
		393.9	3.0(3)		$(M1/E2)$	6
(18^-)	$Y+3467.1$	790.5	9.0(5)	1.2(1)	$E2$	5
(20^-)	$Y+4321.0$	853.9	5.9(4)		$(E2)$	5
(22^-)	$Y+5243.2$	922.2	3.4(3)		$(E2)$	5
(24^-)	$Y+6231.0$	987.8	2.4(2)		$(E2)$	5
(26^-)	$Y+7278.4$	1047.4	<2		$(E2)$	5
(28^-)	$Y+8391.3$	1112.9	<2		$(E2)$	5
(30^-)	$Y+9577.5$	1186.2	<2		$(E2)$	5
(32^-)	$Y+10839.4$	1261.9	<2		$(E2)$	5
(34^-)	$Y+12173.8$	1334.4	<2		$(E2)$	5
(36^-)	$Y+(13584)$	(1410)	<2		$(E2)$	5
		Band 5: $\pi h_{11/2}\nu(d_{3/2}/s_{1/2})$, $\alpha=1$				
(7^-)	$Y+240.9$	89.0	[e]		$M1/E2$	5
(9^-)	$Y+545.3$	304.4	11.1(7)	1.0(1)	$E2$	5
		157.5	11.1(7)	0.7(1)	$M1/E2$	5
		283.2	4.2(4)		$(E2)$	6
		180.6	14.2(7)	0.8(1)	$M1/E2$	6
(11^-)	$Y+985.1$	439.8	25(1)	1.03(9)	$E2$	5
		196.9	3.5(3)		$(M1/E2)$	5
		424.0	11.4(6)	0.9(1)	$E2$	6
(13^-)	$Y+1546.6$	561.5	26(1)	1.0(1)	$E2$	5
(15^-)	$Y+2212.8$	666.2	24(1)	1.1(1)	$E2$	5

TABLE I. *(Continued.)*

I_i^{π} [a]	E_{level} (keV)	E_γ (keV)[b]	I_γ[c]	DCO	Multipolarity	Band$_f$[d]
(17^-)	Y+2957.9	745.1	15.5(8)	1.1(1)	$E2$	5
(19^-)	Y+3761.7	803.8	11.7(6)	1.2(1)	$E2$	5
(21^-)	Y+4632.5	870.8	6.2(4)	1.1(1)	$E2$	5
(23^-)	Y+5597.1	964.6	5.0(3)		$(E2)$	5
(25^-)	Y+6669.0	1071.9	3.0(3)		$(E2)$	5
(27^-)	Y+7861.1	1192.1	<2		$(E2)$	5
(29^-)	Y+9122.8	1261.7	<2		$(E2)$	5
(31^-)	Y+10419.7	1296.9	<2		$(E2)$	5
(33^-)	Y+(11774)	(1354)	<2		$(E2)$	5
		Band 6: $\pi h_{11/2}\nu d_{5/2}$, α=0				
(8^-)	Y+364.5	102.2	6.0(3)		$(M1/E2)$	6
		123.8	19(1)	0.52(5)	$M1/E2$	5
		248.1	9.9(5)	0.57(8)		
(10^-)	Y+750.9	386.4	20(1)	1.00(7)	$E2$	6
		189.5	11.0(6)	0.51(5)	$M1/E2$	6
		206.3	9.0(6)		$(M1/E2)$	5
(12^-)	Y+1272.5	521.6	24(1)	1.06(9)	$E2$	6
		257.1	11.4(6)	0.48(5)	$M1/E2$	6
(14^-)	Y+1906.7	634.2	22(1)	0.99(7)	$E2$	6
		307.4	5.8(4)	0.4(1)	$M1/E2$	6
(16^-)	Y+2627.9	721.2	15.8(8)	1.00(6)	$E2$	6
		344.7	2.8(2)		$(M1/E2)$	6
(18^-)	Y+3411.3	783.4	10.7(6)	0.94(9)	$E2$	6
		368.1	<2		$(M1/E2)$	6
(20^-)	Y+4241.3	830.0	6.4(4)	1.0(1)	$E2$	6
(22^-)	Y+5154.1	912.8	3.1(3)		$(E2)$	6
(24^-)	Y+6180.6	1026.5	2.4(2)		$(E2)$	6
(26^-)	Y+7316.9	1136.3	<2		$(E2)$	6
(28^-)	Y+8547.0	1230.1	<2		$(E2)$	6
(30^-)	Y+9815.8	1268.8	<2		$(E2)$	6
(32^-)	Y+(11115)	(1299)	<2		$(E2)$	6
		Band 6: $\pi h_{11/2}\nu d_{5/2}$, α=1				
(7^-)	Y+262.4	110.9	[e]	0.53(7)	$M1/E2$	5
(9^-)	Y+561.5	299.1	11.1(6)	0.91(9)	$E2$	6
		197.0	12.6(6)	0.49(4)	$M1/E2$	6
		320.8	<2		$(E2)$	5
		173.7	6.9(4)	0.72(8)	$M1/E2$	5
(11^-)	Y+1015.3	453.8	12.2(6)	1.0(1)	$E2$	6
		264.2	16.0(8)	0.44(4)	$M1/E2$	6
		470.4	4.5(4)		$(E2)$	5
		226.7	6.4(5)		$(M1/E2)$	5
(13^-)	Y+1599.1	583.8	15.8(8)	0.92(9)	$E2$	6
		326.6	6.8(4)	0.41(4)	$M1/E2$	6
		280.8	3.0(2)		$(M1/E2)$	5
(15^-)	Y+2283.1	684.0	17.7(9)	1.06(7)	$E2$	6
		376.7	5.3(3)	0.37(8)	$M1/E2$	6
(17^-)	Y+3042.7	759.6	9.4(5)	1.1(1)	$E2$	6
		415.0	2.1(4)		$(M1/E2)$	6
(19^-)	Y+3861.7	819.0	6.5(4)		$(E2)$	6
		449.9	<2		$(M1/E2)$	6
(21^-)	Y+4731.8	870.1	3.5(3)		$(E2)$	6
		490	<2		$(M1/E2)$	6
(23^-)	Y+5696.6	964.8	2.3(2)		$(E2)$	6

TABLE I. *(Continued.)*

I_i^{π} [a]	E_{level} (keV)	E_γ (keV)[b]	I_γ[c]	DCO	Multipolarity	Band$_f$[d]
(25^-)	Y+6778.5	1081.9	<2		$(E2)$	6
(27^-)	Y+7948.9	1170.4	<2		$(E2)$	6
		Band 7: $\pi g_{9/2}\nu h_{11/2}$, α=0				
(10^-)	Z+242.4	242.4	[e]		$(M1/E2)$	7
(12^-)	Z+792.3	549.9	8.1(6)		$(E2)$	7
		285.0	4.7(3)		$(M1/E2)$	7
(14^-)	Z+1416.5	624.2	9.3(6)		$(E2)$	7
		320.6	2.5(2)		$(M1/E2)$	7
(16^-)	Z+2109.1	692.6	9.9(6)		$(E2)$	7
		354.9	<2		$(M1/E2)$	7
(18^-)	Z+2868.8	759.7	6.6(4)		$(E2)$	7
		388	<2		$(M1/E2)$	7
(20^-)	Z+3694.9	826.1	4.2(3)		$(E2)$	7
(22^-)	Z+4587.6	892.7	3.3(3)		$(E2)$	7
(24^-)	Z+5552.8	965.2	2.2(2)		$(E2)$	7
(26^-)	Z+6596.3	1043.5	<2		$(E2)$	7
(28^-)	Z+7720.4	1124.1	<2		$(E2)$	7
(30^-)	Z+8924.0	1203.6	<2		$(E2)$	7
(32^-)	Z+10205.7	1281.7	<2		$(E2)$	7
(34^-)	Z+11560.1	1354.4	<2		$(E2)$	7
(36^-)	Z+(12977)	(1417)	<2		$(E2)$	7
		Band 7: $\pi g_{9/2}\nu h_{11/2}$, α=1				
(9^-)	Z					
(11^-)	Z+507.5	507.5	8.4(8)		$(E2)$	7
		264.9	7.2(4)		$(M1/E2)$	7
(13^-)	Z+1095.7	588.2	10.4(6)		$(E2)$	7
		303.3	3.9(3)		$(M1/E2)$	7
(15^-)	Z+1754.2	658.5	10.1(6)		$(E2)$	7
		337.7	2.4(2)		$(M1/E2)$	7
(17^-)	Z+2480.6	726.4	10.5(6)		$(E2)$	7
		371.8	<2		$(M1/E2)$	7
(19^-)	Z+3275.3	794.7	5.6(3)		$(E2)$	7
(21^-)	Z+4133.3	858.0	3.4(3)		$(E2)$	7
(23^-)	Z+5061.8	928.5	2.2(2)		$(E2)$	7
(25^-)	Z+6065.3	1003.5	<2		$(E2)$	7
(27^-)	Z+7150.0	1084.7	<2		$(E2)$	7
(29^-)	Z+8315.9	1165.9	<2		$(E2)$	7
(31^-)	Z+9558.2	1242.3	<2		$(E2)$	7
(33^-)	Z+10876.5	1318.3	<2		$(E2)$	7
(35^-)	Z+12263.2	1386.7	<2		$(E2)$	7
(37^-)	Z+(13722)	(1459)	<2		$(E2)$	7

[a]Spin and parity of the initial state.
[b]Uncertainties in E_γ are 0.2 keV for most transitions except for relatively weak transitions, which are 0.5 keV.
[c]Relative intensity of the transition, where $I_\gamma(134)\equiv 100$.
[d]Band where the final state is located.
[e]Intensity could not be determined.
[f]Unresolved doublet.

1. This sequence was also identified in the $A=128$ matrix from the ORNL data, and a sample spectrum is shown in Fig. 2(a). In addition, from a gate on the strongest and cleanest transitions for band 1 in the γ vs charged particle matrix, the band could be positively associated with the emission of three protons. Thus, an unequivocal assignment of band 1 to ^{128}Pr can be made as it is the only mass 128 nucleus to result from a $3pXn$ channel in the given reaction. Band 1 was extended from $I=(30^+)$ [14] to $(37^+)\hbar$ in the Gammasphere data as seen in the inset of Fig. 2(a). The intensity of

TABLE II. Data for levels and γ rays in ^{126}Pr.

I_i^{π} [a]	E_{level} (keV)	E_γ (keV)[b]	I_γ [c]	DCO	Multipolarity
		Band 1: $\pi h_{11/2}\nu h_{11/2}$, $\alpha=0$			
(8^+)	$X+105.5$	105.5	[d]	0.41(7)	$M1/E2$
(10^+)	$X+415.9$	310.4	28(3)		$(E2)$
		167.4	99(8)	0.55(7)	$M1/E2$
(12^+)	$X+851.8$	435.9	60(5)	1.0(1)	$E2$
		225.5	68(5)	0.48(7)	$M1/E2$
(14^+)	$X+1409.5$	557.7	58(5)	1.0(1)	$E2$
		283.7	34(3)	0.47(8)	$M1/E2$
(16^+)	$X+2080.4$	670.9	53(5)	1.1(2)	$E2$
		343.5	26(2)		$(M1/E2)$
(18^+)	$X+2852.9$	772.5	43(4)		$(E2)$
		403.4	13(1)		$(M1/E2)$
(20^+)	$X+3715.3$	862.4	29(3)		$(E2)$
		463	8(1)		$(M1/E2)$
(22^+)	$X+4663.3$	948.0	22(2)		$(E2)$
(24^+)	$X+5700.9$	1037.6	13(1)		$(E2)$
(26^+)	$X+6839$	1138	7(1)		$(E2)$
(28^+)	$(X+8085)$	(1246)	<5		$(E2)$
		Band 1: $\pi h_{11/2}\nu h_{11/2}$, $\alpha=1$			
(9^+)	$X+248.6$	248.4	26(3)		$(E2)$
		143.1	$\equiv 100$	0.51(5)	$M1/E2$
(11^+)	$X+626.4$	377.8	41(4)	1.0(1)	$E2$
		210.6	82(7)	0.42(5)	$M1/E2$
(13^+)	$X+1125.9$	499.5	49(4)	0.9(1)	$E2$
		273.8	44(4)	0.41(6)	$M1/E2$
(15^+)	$X+1737.5$	611.6	56(5)	1.2(2)	$E2$
		327.4	30(3)		$(M1/E2)$
(17^+)	$X+2449.9$	712.4	52(5)		$(E2)$
		369.1	25(2)		$(M1/E2)$
(19^+)	$X+3251.9$	802.0	44(4)		$(E2)$
		399.1	10(1)		$(M1/E2)$
(21^+)	$X+4136.4$	884.5	29(3)		$(E2)$
		422	7(1)		$(M1/E2)$
(23^+)	$X+5103.6$	967.2	21(2)		$(E2)$
(25^+)	$X+6158.3$	1054.7	16(2)		$(E2)$
(27^+)	$X+7305.1$	1146.8	10(1)		$(E2)$
(29^+)	$X+8545.1$	1240.0	8(1)		$(E2)$
(31^+)	$X+9865$	1320	<5		$(E2)$
(33^+)	$X+11216$	1351	<5		$(E2)$
		Band 2: $\pi h_{11/2}\nu h_{9/2}$, $\alpha=1$			
(5^+)	$Y+105.5$	105.5	[d]	0.6(1)	
(7^+)	$Y+273.3$	167.8	21(3)	0.94(4)	$E2$
(9^+)	$Y+553.2$	279.9	47(4)	0.92(4)	$E2$
(11^+)	$Y+946.3$	393.1	48(4)	1.00(4)	$E2$
(13^+)	$Y+1445.1$	498.8	47(4)	1.20(5)	$E2$
(15^+)	$Y+2039.6$	594.5	40(3)	1.16(5)	$E2$
(17^+)	$Y+2721.5$	681.9	39(3)	1.04(6)	$E2$
(19^+)	$Y+3485.2$	763.7	30(3)	1.21(6)	$E2$
(21^+)	$Y+4328.7$	843.5	23(2)	1.02(6)	$E2$
(23^+)	$Y+5251.5$	922.8	18(2)	0.99(7)	$E2$
(25^+)	$Y+6254.6$	1003.1	15(2)		$(E2)$
(27^+)	$Y+7337.7$	1083.1	10(1)		$(E2)$
(29^+)	$Y+8499.5$	1161.8	6(1)		$(E2)$
(31^+)	$Y+9738.0$	1238.5	<5		$(E2)$
(33^+)	$Y+11051.5$	1313.5	<5		$(E2)$
(35^+)	$Y+12444.0$	1392.5	<5		$(E2)$
(37^+)	$Y+13923$	1479	<5		$(E2)$
(39^+)	$Y+15500$	1577	<5		$(E2)$
(41^+)	$(Y+17151)$	(1651)	<5		$(E2)$

[a]Spin and parity of the initial state.
[b]Uncertainties in E_γ are 0.2 keV for most transitions except for relatively weak transitions, which are 0.5 keV.
[c]Relative intensity of the transition, where $I_\gamma(143)\equiv 100$.
[d]Intensity could not be determined.

this structure (see Table I) indicates that it is the yrast sequence over the majority of the observed spin region. Parity and spins were assigned based on the proposed configuration described in the following section and the systematics of Liu *et al.* [5], which led to an assignment of 1 $\hbar$ lower than that suggested in Ref. [14]. A more detailed discussion of the spin assignment follows in Sec. II B.

Band 2 is a new doubly decoupled structure, which was found only in the Gammasphere data. Near the bottom of the band, linking transitions to both bands 1 and 3 were observed, as shown in Fig. 1. Indeed, transitions from these latter structures can be observed in the spectrum displayed in Fig. 2(b), which is a sum of many double-gated spectra above the (13^+) level in band 2. The 357-keV transition that feeds the (10^+) state in band 1 has a DCO ratio of 0.6(1) indicating that it has $\Delta I=1$. If a spin of (11^+) is given to the state from which the 357-keV transition depopulates, band 2 would become yrast with respect to band 1 at $I=(15^+)$.

TABLE III. Experimental and calculated relative cross sections for ^{40}Ca+^{92}Mo reaction at $E_{lab}=170$ MeV.

Channel[a]	Nucleus	Experimental relative cross section (%)[b]	Calculated relative cross section (%)[b]	Calculated absolute cross section (mb)
$2pn$	^{129}Nd	40(6)	35.9	48.1
$2p2n$	^{128}Nd	3.0(5)	2.6	3.5
$3p$	^{129}Pr	$\equiv 100$	$\equiv 100$	134
$3pn$	^{128}Pr	30(4)	28.1	37.7
αp	^{127}Pr	<3	4.6	6.2
αpn	^{126}Pr	2(1)	1.9	2.5
$4p$	^{128}Ce	44(2)	47.2	63.2
$4pn$	^{127}Ce	<5	1.1	1.4
$\alpha 2p$	^{126}Ce	77(4)	17.0	22.8

[a]Charged particle emission channel from the ^{132}Sm compound nucleus. p, n, and α denote emitted proton, neutron, and alpha particles, respectively.
[b]Relative cross section with respect to ^{129}Pr.

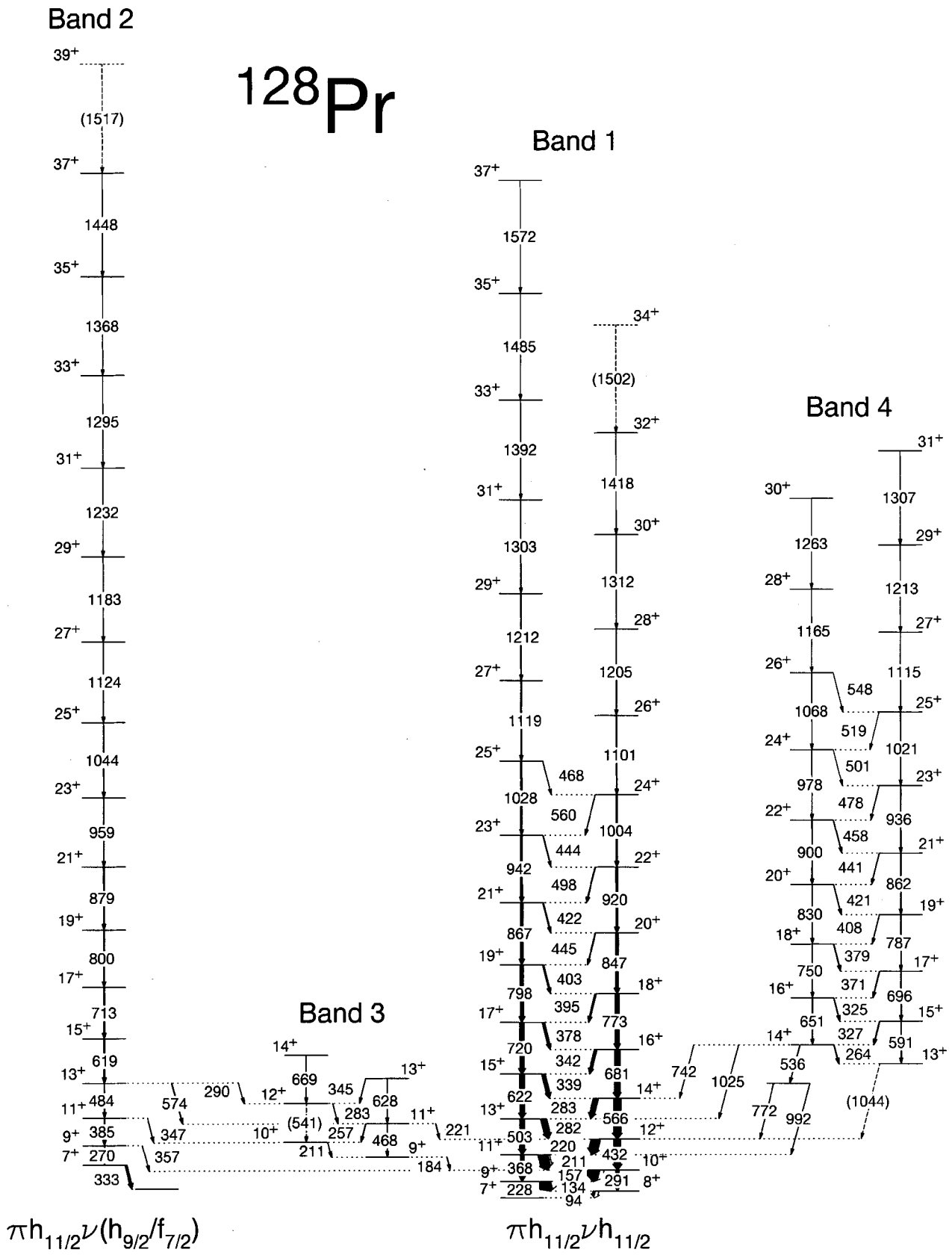

FIG. 1. Partial level scheme of ^{128}Pr, depicting the proposed positive-parity bands. The width of the arrows is proportional to the transition's relative intensity. Tentative transitions and levels are denoted with dashed lines. Configurations for some of the sequences are also provided. All spins and parities are considered tentative.

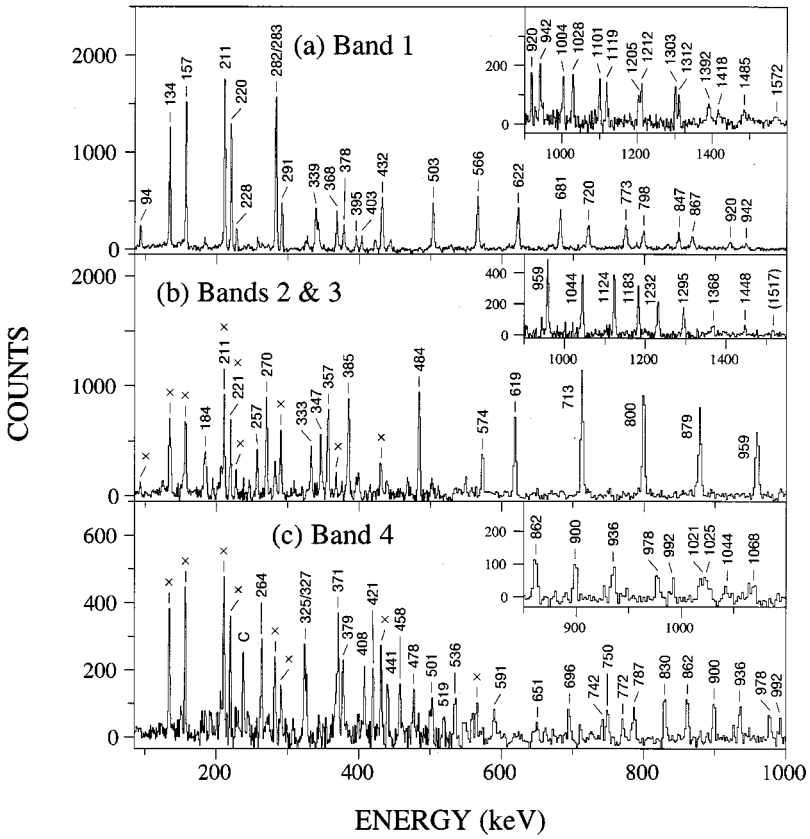

FIG. 2. (a) Spectrum of band 1 in ^{128}Pr. The spectrum was produced by a sum of gates on the 134-, 157-, 211-, 220-, and 282-keV transitions in the $A=128$ matrix from the ORNL experiment. The inset displays the high-energy portion of the band obtained from the Gammasphere data. (b) Spectrum of bands 2 and 3 produced by summing many double-gated coincidence spectra above the (13^+) level. The inset displays the high-energy portion of the band. (c) Spectrum of band 4 obtained from all possible combinations of double gating on most of the $\Delta I=1$ in-band γ rays. The inset displays the high-energy portion of the band. In panels (b) and (c), peaks marked with a $\times$ are transitions from band 1. Peaks denoted with a *C* are contaminant transitions.

However, the intensities of the two structures do not support this assignment. Instead, an $I\rightarrow I+1$ assignment is given to the 357-keV γ ray, which makes band 2 nonyrast at lower spins, but it is nearly yrast at the highest spins. This relative spin assignment is consistent with the observed intensities. The assigned positive parity was based on the configuration assignment (see below), which is consistent with band 2 feeding into other proposed positive-parity states.

The short sequence of new levels labeled as band 3 in Fig. 1 is mainly populated by the feeding transitions from band 2. The 347-keV linking transition from band 2 to band 3 was found to have a DCO ratio of 0.7(1) indicating $\Delta I=1$, while the 574-keV linking transition has a DCO ratio of 0.9(1), which suggests $\Delta I=2$. Thus the relative spin assignments of band 3 could be made as shown in Fig. 1. The 574-keV γ ray is the strongest feed-out transition from band 2, which is likely due to mixing between the $I=(13^+)$ states of these two bands. This mixing confirms the relative spins as well as the fact that band 3 has the same positive parity as band 2.

A weak, strongly coupled structure was observed in the Gammasphere data and has been labeled as band 4 in Fig. 1. A spectrum is provided in Fig. 2(c), which shows that band 4 is in coincidence with band 1. In fact, as shown in Fig. 1, the decay out of band 4 is highly fragmented while feeding into the yrast structure. Unfortunately, due to the weakness of the band, DCO ratios could not be extracted for the linking or in-band transitions. Tentative spin assignments were based on intensity and excitation energy considerations. Since none of the strongly populated, negative-parity bands were found to interact with band 1, band 4 has been given positive parity.

2. Negative-parity bands in ^{128}Pr

The rotational sequences that are suggested to have negative parity are shown in Fig. 3. Figure 4(a) displays a spectrum of a band found in the $A=128$ matrix from the ORNL data. Similar to band 1, the strongest and cleanest transitions were found in coincidence with the emission of three protons. Thus, band 5 (as labeled in Fig. 3) is positively identified in ^{128}Pr, and confirms the assignment of Watson *et al.* [20]. The Gammasphere data allowed for the extension of this structure to high spins as shown in the inset of Fig. 4(a). In addition, a short sequence was found to feed into band 5 at $I=(25^-)$ (see Fig. 3). The signature partner for band 5 was not observed in the ORNL matrix, but could be observed in the Gammasphere cube and a spectrum is displayed in Fig. 4(b). Many transitions in Fig. 4(b) (denoted with an asterisk) are found corresponding to γ rays in band 6, which is the result of a strong interaction between the bands at lower spins (see Fig. 3). Tentative spin assignments were based on an analysis of the proposed configuration and the initial alignment of the band, as described in Sec. III A 2. With the given spin assignment, band 5 was extended from $I=(17^-)$ to (36^-). The strong interaction of bands 5 and 6 indicate that they have the same parity. The in-beam properties of band 6 (see below) strongly suggest a configuration with negative parity; therefore, band 5 is also given negative parity.

The structure labeled as band 6 in Fig. 3 was observed in both the ORNL and ANL data sets. The spectrum provided in Fig. 4(c) came from the Gammasphere cube, which displays

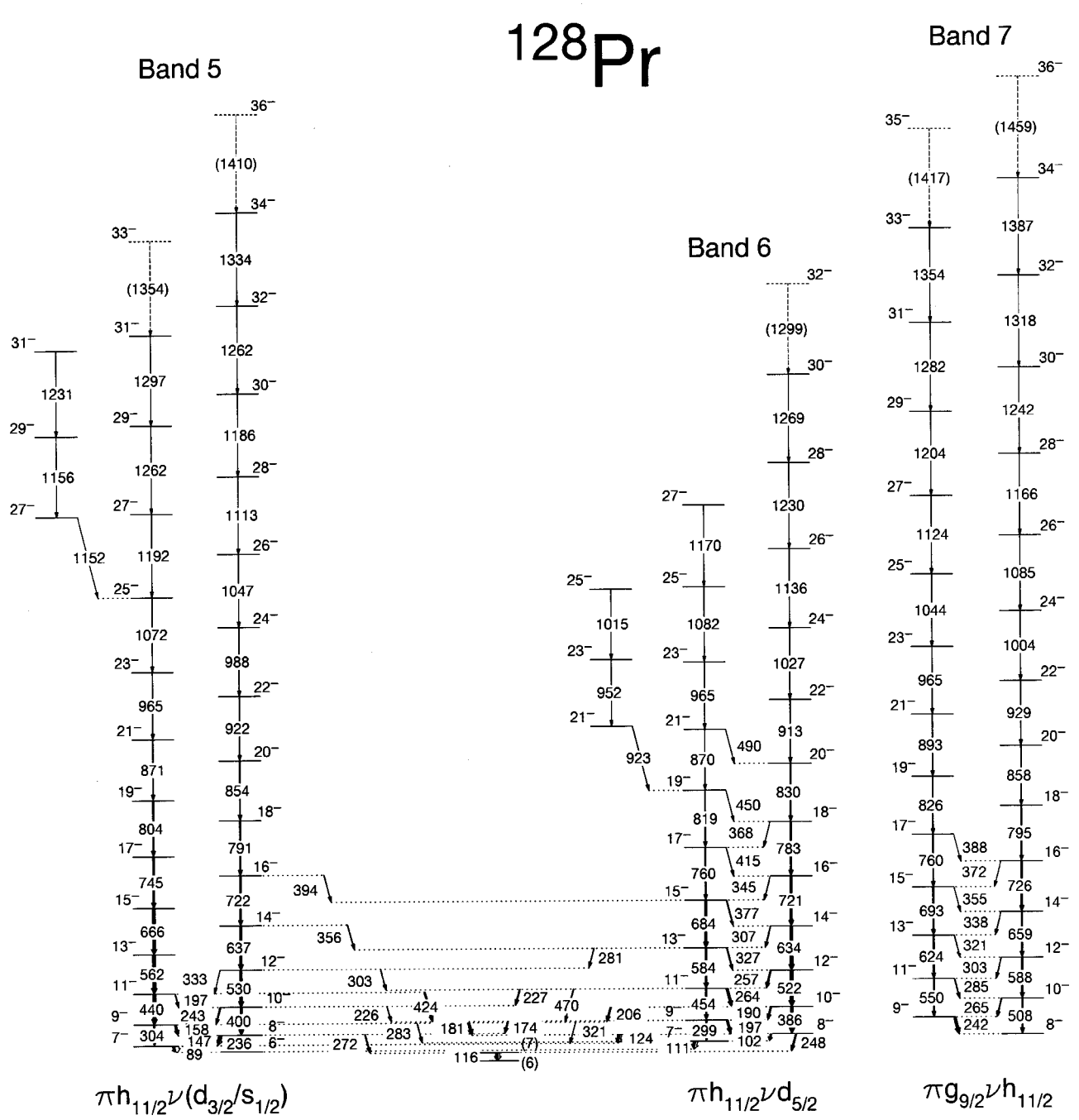

FIG. 3. Partial level scheme of ^{128}Pr, depicting the proposed negative-parity bands. The width of the arrows is proportional to the transition's relative intensity. Tentative transitions and levels are denoted with dashed lines. Configurations for some of the sequences are also provided. All spins and parities are considered tentative.

both signatures of this strongly coupled sequence. Due to the aforementioned interaction between bands 5 and 6, many transitions originating from band 5 are observed in Fig. 4(c) and are denoted with a plus sign. DCO analysis of the linking transitions (see Table I) fix the relative spins of band 6 with respect to band 5. As previously stated, the parity assignment of this structure was based on the proposed configuration discussed below. Band 6 was extended from $I=(16^-)$ to (32^-) and a small sequence of transitions was also observed to feed into the (19^-) state. The (8^-) states in both bands 5 and 6 were found to feed into a state that is depopulated by a 116-keV transition (see Fig. 3). The DCO ratios ($\sim$0.6) of the 272- and 248-keV linking transitions from bands 5 and 6, respectively, indicate that they are dipole transitions with $\Delta I=1$; however, the parity of the $Y+116$-keV state could not be determined.

Band 7 was previously reported by Smith *et al.* [14], but linking transitions to known states could not be established. Unfortunately, this structure was not observed in the ORNL experiment and connecting transitions were not observed in the Gammasphere data. However, the relative intensity of band 7 to band 1 is similar to that reported in Ref. [14], thus

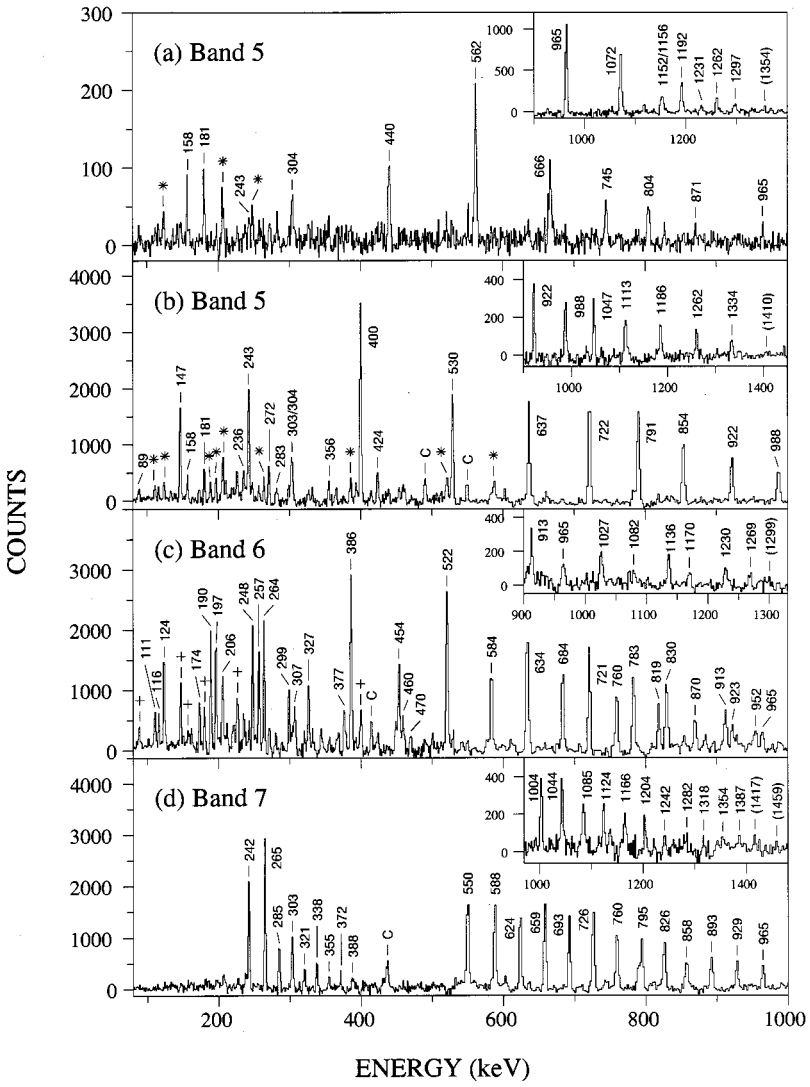

FIG. 4. (a) Spectrum of the $\alpha=1$ signature of band 5 from the $A=128$ mass-gated matrix from transitions in coincidence with 181-, 304-, and 440-keV γ rays. The high-energy inset displays the extension of this signature to high spin from the Gammasphere cube. (b) Spectrum of the $\alpha=0$ signature of band 5 from the Gammasphere data resulting from the sum of double-gated coincidence spectra above the (12^-) level. In panels (a) and (b), peaks marked with an asterisk are transitions originating from band 6. (c) Spectrum of band 6 with the high-energy portion shown in the inset. Transitions originating from band 5 are denoted with a plus sign. (d) Spectrum of band 7 from double gating the 242- and 265-keV γ rays with all coincident $\Delta I=2$ in-band transitions. The inset displays the high-energy γ rays in the band. In panels (b), (c), and (d), peaks labeled with a *C* are contaminant transitions.

suggesting that it is indeed associated with ^{128}Pr. Figure 4(d) displays a spectrum of this sequence where one may notice that none of the previously established transitions in ^{128}Pr can be observed. This fact suggests that the lowest state is likely isomeric with a lifetime that is longer than the prompt coincidence window of ~80 ns. The isomeric state must be the band head of the structure; therefore, the proposed configuration (see below) would give a K^π value and band head spin of (8^-). Band 7 was also extended by 6 $\hbar$ and 4 $\hbar$ in the $\alpha=0$ and 1 signatures, respectively, compared with the observations in Ref. [14].

B. The ^{126}Pr level scheme

Results on ^{126}Pr from these experiments have been published elsewhere [12]; however, a more detailed discussion of the bands shall be addressed in the present work. The $A=126$ matrix from the ORNL experiment was dominated by transitions from the $\alpha 2p$ channel (^{126}Ce [22]). γ rays in coincidence with an α particle and two protons were subtracted from the $A=126$ projection with the resulting spectrum shown in Fig. 5(a). Coincidence gates were set on each of the remaining peaks of Fig. 5(a) in the Gammasphere cube, which contained γ rays associated with the αp channel. A sample spectrum is given in Fig. 5(b) that shows a strongly coupled sequence. This structure was not observed in cubes coincident with the $2p, 3p, 4p, \alpha 2p, 2\alpha p$, or 2α channels, thus confirming that the band results from an αpXn emission. Combining the facts that the band is (i) correlated with mass 126 from the ORNL experiment and (ii) associated with the emission of an α particle and a proton from the ANL experiment, it must be identified with ^{126}Pr. A level scheme for ^{126}Pr is shown in Fig. 6 and this yrast sequence is labeled as band 1.

A comparison of the level energies in the yrast structures of odd-odd $^{126-136}$Pr (including band 1 from both ^{126}Pr and ^{128}Pr) is shown in Fig. 7(a). Similar to the procedure of Liu *et al.* [5], the $I=(10^+)$ state is set to 0 keV such that the relative level energies for higher-lying states may be compared. A smooth systematic trend may be observed in the energy levels with our proposed spins for band 1 in ^{126,128}Pr. However, Petrache *et al.* [23] recently suggested that the spins of these bands should be raised by two units of $\hbar$ in comparison with our assignments. An interacting-boson-

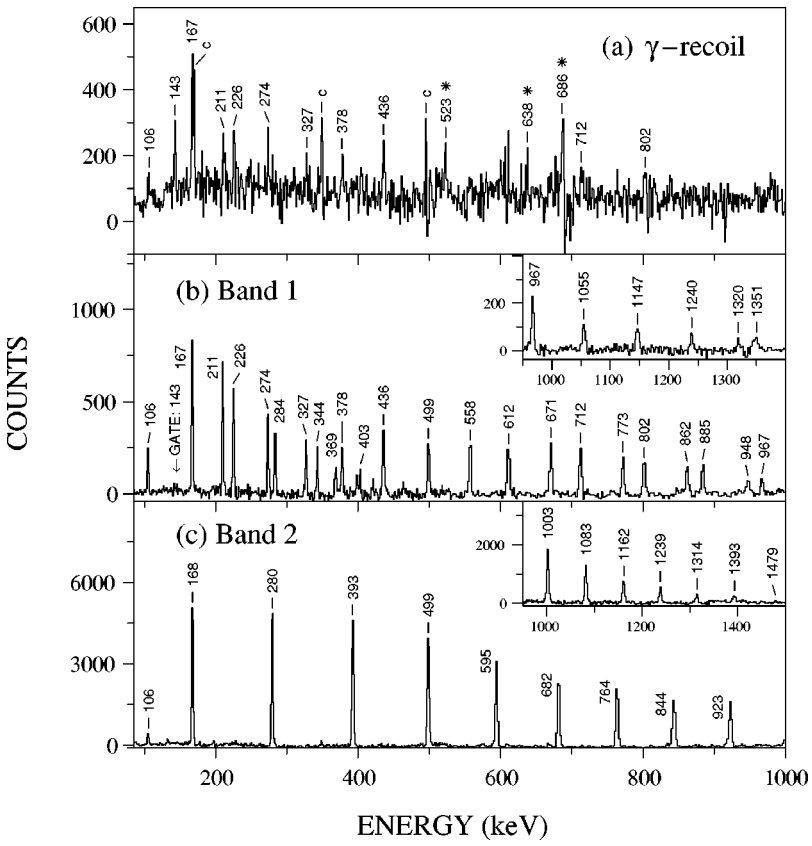

FIG. 5. (a) Spectrum of transitions in coincidence with $A=126$ recoils after a fraction of the γ rays coincident with the $\alpha 2p$ channel (^{126}Ce) was subtracted. The three strongest transitions in ^{126}Ce are observed in the spectrum and are labeled with a *C*. Peaks marked with an asterisk could not be identified with a band structure. (b) Spectrum of band 1 in ^{126}Pr from the Gammasphere experiment produced by summing over all the double-gated coincidence spectra between the 143-keV transitions and the $\Delta I=1$ γ rays below the (18^+) level. The inset is the high-energy portion of the $\alpha=1$ signature. (c) Spectrum of band 2 in ^{126}Pr from the Gammasphere experiment. A sum over all possible double gates of the transitions depopulating the states between (9^+) to (21^+) was used to produce the spectrum. The inset shows the high-energy portion of the band.

fermion-fermion calculation and comparison of alignments with the yrast band in ^{130}Pr were used to support their argument. Assigning spins to odd-odd bands is always difficult, but this suggestion would cause a severe discontinuity in the energy level systematics (see Fig. 9 in Ref. [23]) between the $N=71$ and 69 nuclei. Energy level systematics from the ground-state, $\nu h_{11/2}$, and $\pi h_{11/2}$ bands in even-even Ce ($Z=58$), odd-*A* Ce, and odd-*A* Pr nuclei, respectively, are shown in Fig. 7(b). The $I=9/2^-$ and $11/2^-$ states in the $\nu h_{11/2}$ and $\pi h_{11/2}$ bands, respectively, were set to 0 keV in order to do the comparison. No irregularities are found in any of the nearby nuclei as seen in Fig. 7(b); therefore, it would be difficult to understand why a discontinuity in odd-odd Pr nuclei would exist. Instead, we suggest that our spin assignments are more consistent with the experimental data of nearby nuclei, and additional support is also given in Sec. III C based on relative alignments with ^{127}Pr.

A decoupled sequence, shown in Fig. 5(c), was observed in the Gammasphere data and associated with the αpXn channel in a similar manner as described for band 1 in ^{126}Pr. The intensity of this structure was found to be larger than either of the yrast bands in ^{125}Pr [24] ($\alpha p2n$ channel) or ^{127}Pr [25] (αp channel). Thus, it is tentatively assigned to the αpn channel and is included as band 2 in the level scheme of ^{126}Pr in Fig. 6. Band 2 was not identified in the ORNL experiment as the population intensity was likely below the experimental sensitivity level. Therefore, we cannot completely rule out the possibility that band 2 belongs to another nucleus. DCO ratios indicate that the in-band transitions are of $E2$ character, while the 106-keV γ ray is a dipole transition. Thus, it has been assumed that this low-energy transition is a decay out of the band. The tentative parity and spin assignments are based on the given configuration (see below) and energy systematics of similar bands found in heavier Pr nuclei.

III. CONFIGURATION ASSIGNMENTS

In the neighboring odd-Z ^{127,129}Pr [25,26] nuclei, the sequence based on the $h_{11/2}$ low-K proton ([541]3/2) is found to be much lower in energy than any other configuration. However, structures based on the $d_{5/2}/g_{7/2}$[411]3/2 and $g_{9/2}$[404]9/2 protons are also observed. In the nearby odd-N $^{129}_{60}$Nd [27] nucleus, four bands originating from the $h_{11/2}$[523]7/2,$h_{9/2}/f_{7/2}$[541]1/2,$d_{3/2}/s_{1/2}$[411]1/2, and $d_{5/2}$[402]5/2 orbitals were seen. Thus, combinations of these protons and neutrons were primarily considered for the configurations of the bands in ^{126,128}Pr. Band characteristics such as alignments, band crossings, $B(M1)/B(E2)$ ratios, and signature splitting were investigated in order to assign the proper configurations.

A. Alignments and band crossings in ^{128}Pr

1. Positive-parity bands

An alignment plot of the structures in ^{128}Pr is shown in Fig. 8. The same Harris parameters of $\mathcal{J}_0=18\hbar^2/\mathrm{MeV}$ and $\mathcal{J}_1=22\hbar^4/\mathrm{MeV}^3$ employed for ^{127}Pr [25] were used to subtract the core angular momentum. Cranked shell model (CSM) [28] calculations were performed to help interpret the

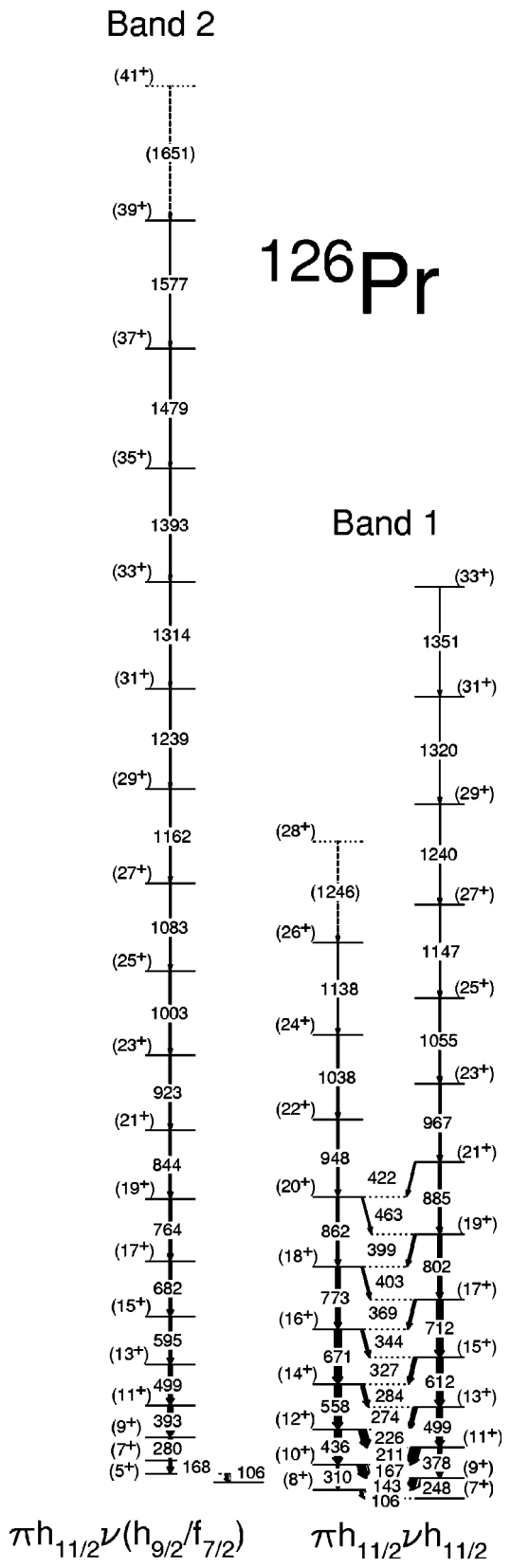

FIG. 6. Level scheme of ^{126}Pr. The width of the arrows is proportional to the transition's relative intensity. Tentative transitions and levels are denoted with dashed lines. Configurations for the sequences are also provided.

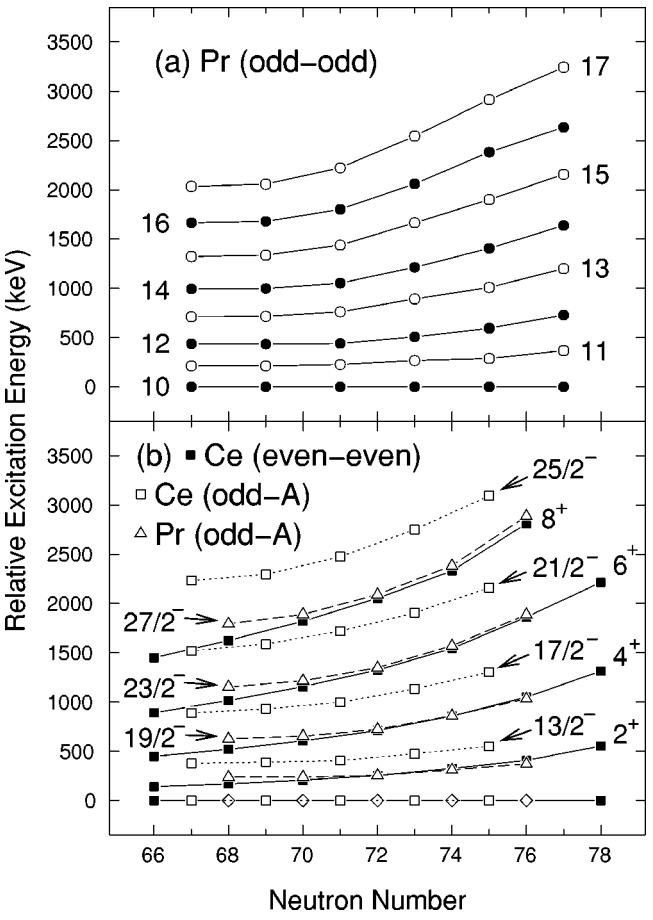

FIG. 7. (a) Energy level systematics of yrast bands in odd-odd Pr nuclei. Following the procedure of Liu *et al.* [5], the $I=(10^+)$ state was set to 0 keV such that the relative level energies for higher-lying states may be compared. (b) Energy level systematics of the ground-state bands in even-even Ce (filled squares), $\alpha=+1/2$ signature of the $\nu h_{11/2}$ band in odd-A Ce (open squares), and the $\pi h_{11/2}$ band in odd-A Pr (open triangles). The $9/2^-$ and $11/2^-$ states in the $\nu h_{11/2}$ and $\pi h_{11/2}$ bands, respectively, were set to 0 keV.

observed crossings and are shown in Fig. 9. Deformation parameters were taken from a total Routhian surface (TRS) calculation.

A large initial alignment ($\sim 6\hbar$) is observed for band 1 in Fig. 8(a) and an alignment gain of 5–6 $\hbar$ is found in both signatures at $\hbar\omega \approx 0.41$ MeV. The $\pi(d_{5/2}/g_{7/2})$ bands in ^{127,129}Pr experience an alignment gain of $\sim 10\hbar$ just below 0.3 MeV, which is due to the breaking of the lowest pair of $h_{11/2}$ protons from their time-reversed orbits and aligning their angular momenta along the nuclear spin axis. This is often referred to as the E_pF_p band crossing and one may see that the CSM predicts that this will occur at 0.3 MeV in Fig. 9(a). However, no such crossing is found in band 1 of ^{128}Pr, indicating that an $h_{11/2}$ proton must be involved in the configuration to Pauli block the E_pF_p crossing. The alignment gain near 0.4 MeV is attributed to the second $h_{11/2}$ proton crossing (F_pG_p), which is lower than the CSM predicted value of ~ 0.48 MeV [see Fig. 9(a)]. In addition, the alignment of the lowest $h_{11/2}$ neutrons (known as the EF crossing), which is observed in some of the other bands in ^{128}Pr

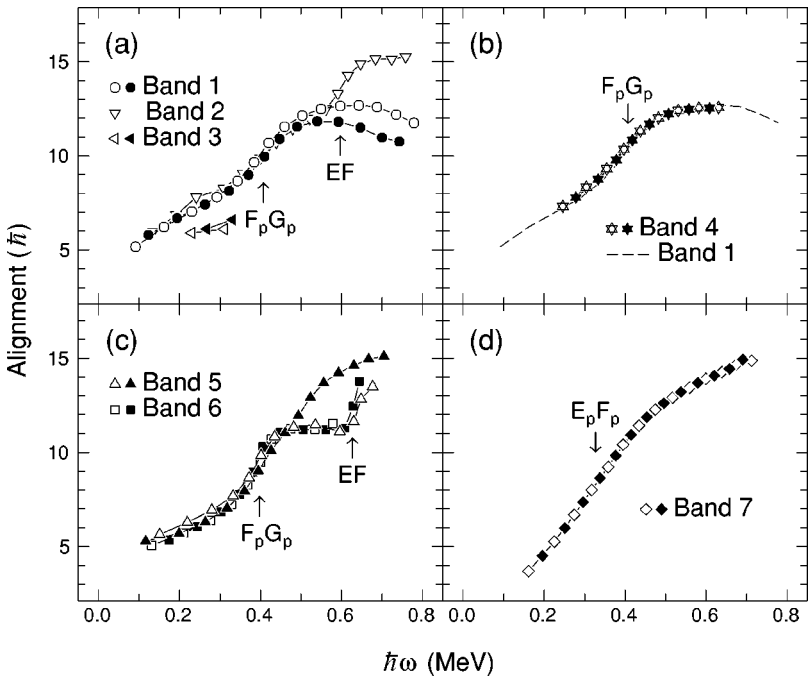

FIG. 8. Alignments for the bands in ^{128}Pr. Harris parameters of $\mathcal{J}_0 = 18\hbar^2/\mathrm{MeV}$ and $\mathcal{J}_1 = 22\hbar^4/\mathrm{MeV}^3$ were used to subtract the angular momentum of the rotating core. Observed crossings are designated in the figure. Filled (empty) symbols denote the $\alpha=0$ (1) sequence.

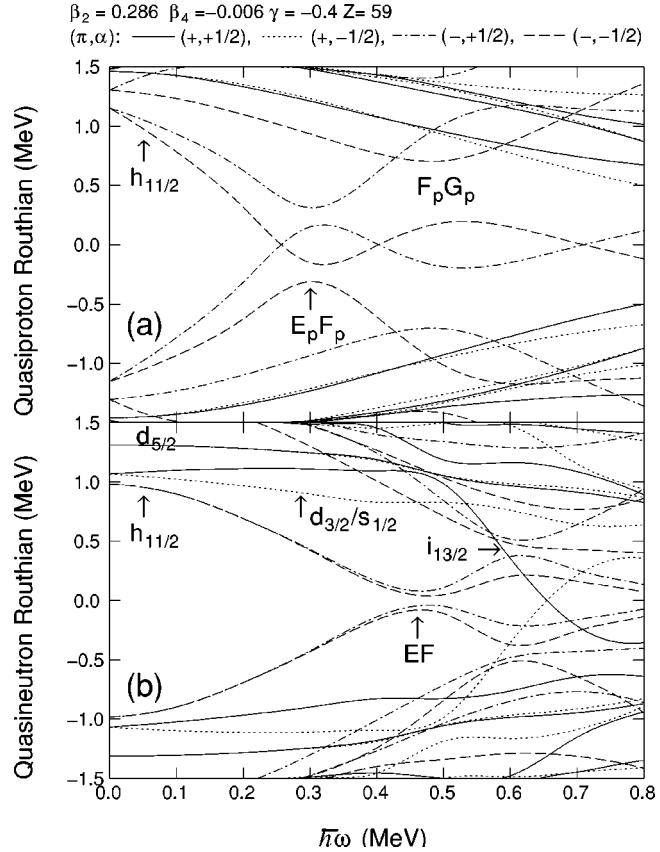

FIG. 9. Cranked shell model calculated (a) quasiproton and (b) quasineutron Routhians. The deformation parameters (shown at the top of figure) were determined by TRS calculations. Interpretation of the lines is displayed at the top of the figure. Some of the lowest-lying lines are designated with their configuration when $\hbar\omega=0$ MeV.

near 0.6 MeV (see below), is blocked in band 1. Hence, the $\pi h_{11/2}\nu h_{11/2}$ configuration has been assigned to this structure. The Gallagher-Moszkowski rule [29] states that when both the valence proton and neutron in an odd-odd nucleus originate from shells with parallel spin angular momenta, the K of the band is equal to the sum of K values from the unpaired nucleons. Such is the case for the $\pi h_{11/2}\nu h_{11/2}$ configuration, and thus $K^\pi = 5^+$ has been assumed for band 1.

The fact that band 2 is a decoupled sequence indicates that a low-K proton and neutron are likely responsible for the band. A blocking of the E_pF_p crossing and the observation of the F_pG_p crossing at $\hbar\omega \approx 0.42$ MeV in band 2 [see Fig. 8(a)] implies the $h_{11/2}$ proton is involved. A crossing is observed at 0.60 MeV, which we associate with the EF neutron alignment. CSM calculations predict this neutron crossing to occur near 0.47 MeV [see Fig. 9(b)]; however, delayed EF alignments have also been observed in $N \approx 70$ Ce nuclei [30]. The force(s) responsible for this delay is likely producing the same effect in ^{128}Pr. In ^{130}Pr [31], the $\pi h_{11/2}\nu(h_{9/2}/f_{7/2})$ band is found to lie high in energy with respect to the yrast sequence at low spin, but approaches the yrast line at the highest spin. This is due to a higher deformation in the $\pi h_{11/2}\nu(h_{9/2}/f_{7/2})$ sequence as measured by Kondev *et al.* [31]. Band 2 behaves in a very similar manner, thus this same configuration is assigned to the decoupled structure in ^{128}Pr. Depending on whether the mixed parentage of the [541]1/2 orbital is more dominantly $f_{7/2}$ or $h_{9/2}$, a parallel or antiparallel combination of the spin angular momenta is possible. Thus, this structure may have a K^π of either 2^+ or 1^+, respectively.

Although band 3 is a short sequence, it is possible to suggest a configuration assignment based on the observed properties. Figure 8(a) shows that this band has a large alignment ($\sim 5\hbar$), but is $\sim 1\hbar$ less than that seen in band 1. The large alignment strongly suggests that the $h_{11/2}$ proton is involved in the configuration of band 3. As the structure likely

has positive parity, a negative-parity neutron must be coupled with the $h_{11/2}$ proton. The negative-parity neutron orbitals nearest to the Fermi surface are [523]7/2 and [541]1/2; however, only the [523]7/2 would produce a strongly coupled sequence as band 3 appears to be. In ^{129}Pr [26], the unfavored signature of the $\pi h_{11/2}$ band has been observed to have $\sim 1\hbar$ less in alignment than the favored signature. This is similar to the difference between bands 1 and 3 in Fig. 8(a). Therefore, band 3 is suggested to have the $\pi h_{11/2} \nu h_{11/2}$ configuration, where the unfavored signature of the $h_{11/2}$ proton is involved. Observed bands based on unfavored couplings of nucleons in odd-odd nuclei are rare, but have been seen as in ^{164}Tm [3]. With the unfavored signature of the proton, an opposite *K* coupling, with respect to band 1, must be used; therefore, the difference between the *K* values suggests $K^{\pi}=2^{+}$ for band 3. This assignment offers a reason for why band 2 favors feeding into band 3, where $\Delta K=0$ or 1, versus feeding into band 1, where $\Delta K=3$ or 4 is classically forbidden.

The alignment of band 4 has been plotted in Fig. 8(b) along with the $\alpha=1$ signature of band 1. One may see the striking similarity between these bands as they have nearly the same amount of alignment throughout the observed frequency range of band 4. The blocking of the E_pF_p and EF crossings and the observation of the F_pG_p crossing indicate that the $h_{11/2}$ proton and neutron are involved in the configuration of this structure. As band 4 is not observed until high excitation energy, it is likely based on four quasiparticles. The fact that bands 1 and 4 have nearly the same alignment suggests that the other two nucleons have nearly zero alignment associated with them. The $B(M1)/B(E2)$ ratios discussed in Sec. III B offer more insight as regards which two quasiparticles are coupled to the $h_{11/2}$ nucleons to form band 4.

2. Negative-parity bands

A blocking of the E_pF_p crossing is once again observed in band 5, along with the observation of the F_pG_p crossing at $\hbar\omega \approx 0.39$ MeV [see Fig. 8(c)]. Thus, the $h_{11/2}$ proton is associated with this structure. Significant signature splitting is seen below spin (20^{-}) in this band, which suggests that a low-*K* neutron is coupled to the $h_{11/2}$ proton. As the only low-*K* orbital near the Fermi surface (other than [541]1/2 that is involved in the configuration of band 2) is the [411]1/2 neutron, band 5 is assigned $\pi h_{11/2} \nu(d_{3/2}/s_{1/2})$ and $K^{\pi}=1^{-}$ or 2^{-}. Nearly $5\hbar$ of alignment is associated with the $h_{11/2}$ proton [25], while very little alignment is observed for the [411]1/2 neutron [27]. Therefore, a band head spin of (6^{-}) was tentatively assigned for band 5 such that its initial alignment at low frequency (<0.3 MeV) is $\sim 0.5\ \hbar$ higher than the $\pi h_{11/2}$ band in ^{127}Pr. The $\alpha=1$ signature [open triangles in Fig. 8(c)] experiences another crossing above $\hbar\omega = 0.6$ MeV, which is similar to those found in bands 2 and 6. All of these crossings are interpreted as the EF neutron alignments as this is the next crossing available for these configurations according to the CSM calculations of Fig. 9. The nature of the alignment gain observed in the $\alpha=0$ signature near 0.5 MeV will be discussed in Sec. V.

The alignment for band 6 is nearly identical to the $\alpha=1$ signature of band 5, as one can see in Fig. 8(c). The F_pG_p and EF crossings are observed for $\hbar\omega \approx 0.39$ and >0.6 MeV, respectively, in both bands. As little signature splitting is found for band 6, a high-*K* neutron is likely coupled with the $h_{11/2}$ proton. Since the [523]7/2 neutron has already been associated with bands 1 and 3, it was not considered for band 6. The $d_{5/2}$[402]5/2 orbital is the next closest high-*K* orbital to the $N=69$ Fermi surface as seen in Fig. 9(b) and observed in ^{129}Nd [27]. Indeed, an excellent agreement between theoretical $B(M1)/B(E2)$ values for the $\pi h_{11/2} \nu d_{5/2}$ configuration and the experimentally determined transition strength ratios for band 6 is found (see below). Therefore, the $\pi h_{11/2} \nu d_{5/2}$ assignment is given to band 6, which suggests that the structure has negative parity and $K^{\pi}=4^{-}$.

Band 7 was previously identified as the $\pi g_{9/2} \nu h_{11/2}$ configuration by Smith *et al.* [14]. The lower initial alignment seen in Fig. 8(d) and the identification of the E_pF_p crossing near 0.3 MeV indicate a proton other than the $h_{11/2}$ proton is involved. Bands based on the $g_{9/2}$ proton have been observed in many Pr nuclei [14,32], and it would most likely couple with the yrast $h_{11/2}$ neutron. Confirmation of this assignment can be observed in Sec. III B, where the theoretical and experimental $B(M1)/B(E2)$ ratios are in good agreement. The lack of decays from higher spin states in band 7 indicates that it does not mix with the other structures, resulting from a rather pure $\pi g_{9/2} \nu h_{11/2}$ configuration. The $K^{\pi}=8^{-}$ of this configuration classically forbids decay to any of the other structures in ^{128}Pr. Thus, a relatively long lifetime of the band head state may be expected.

B. $B(M1)/B(E2)$ ratios for ^{128}Pr

The inband $B(M1)/B(E2)$ ratios were determined by the standard formula

$$\frac{B(M1{:}I\rightarrow I-1)}{B(E2{:}I\rightarrow I-2)} = 0.693 \frac{E_{\gamma}^{5}(I\rightarrow I-2)}{E_{\gamma}^{3}(I\rightarrow I-1)} \frac{1}{\lambda(1+\delta^{2})} \left(\frac{\mu_N}{e\mathrm{b}}\right)^{2},$$

where λ is the branching ratio and E_{γ} is in MeV. Mixing ratios (δ) were estimated from the rotational model and assumed pure *K* [33]. Figure 10 displays the results for ^{128}Pr, along with theoretical calculations based on the extended formalism [34] of the geometrical model from Dönau [35] and Frauendorf [36]. Parameters used in the calculations of $M1$ strengths are summarized in Table IV and a quadrupole moment of $Q_0=4.9\ e$b was assumed from a TRS predicted deformation of $\beta_2=0.29$. The collective gyromagnetic ratio was determined by $g_R=Z/A$, and the g_K values were calculated using a Woods-Saxon potential [37]. Alignment values (i_x) were determined from the initial alignments in the neighboring odd-*A* nuclei ^{127}Pr [25] and ^{129}Nd [27].

In Fig. 10(a), the $B(M1)/B(E2)$ ratios for band 1 are found to lie consistently between $1.0(\mu_N/e\mathrm{b})^2$ and $1.5(\mu_N/e\mathrm{b})^2$. The solid curve in panel (a) denotes the calculated ratios for the $\pi h_{11/2} \nu h_{11/2}$ configuration. It is apparent that the theoretical calculations do not give a good fit to the data for most of the observed spin region. However, one may notice that the experimental points between $I=14$ to 20 lie

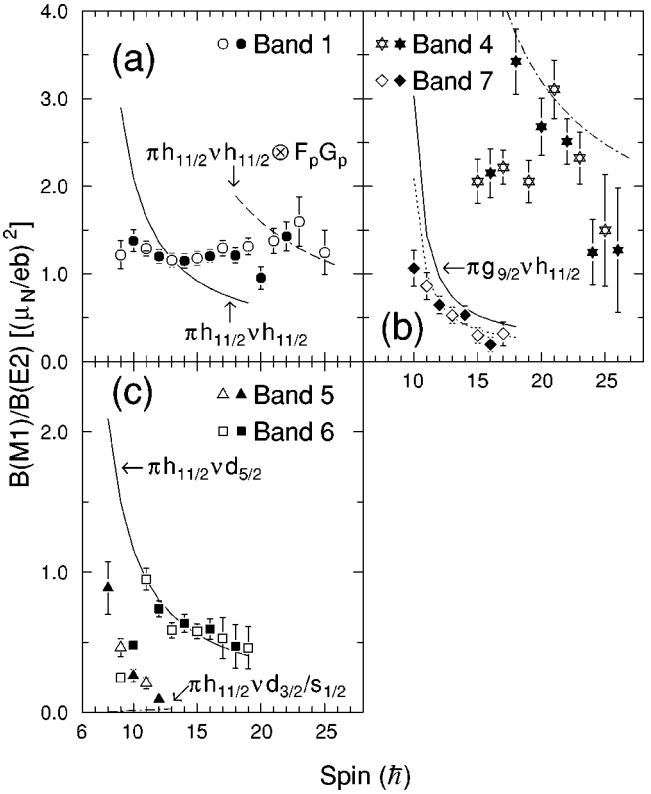

FIG. 10. $B(M1)/B(E2)$ ratios for bands 1, 4, 5, 6, and 7 in ^{128}Pr. Filled (empty) symbols represent the experimental values for the $\alpha=0$ (1) sequence. Calculated values (as described in the text) are shown as lines.

between the calculated $\pi h_{11/2}\nu h_{11/2}$ and $\pi h_{11/2}\nu h_{11/2}\otimes F_pG_p$ [dashed line in Fig. 10(a)] values. This may indicate that a strong interaction between the two- and four-quasiparticle bands exists, which would cause such discrepancies.

Figure 10(b) displays the transition strength ratios for bands 4 and 7. As previously mentioned, band 4 likely has four quasiparticles, where the $h_{11/2}$ proton and neutron are involved. If the other two quasiparticles were nearby protons, namely, $d_{5/2}/g_{7/2}$ and $g_{9/2}$, the calculated $B(M1)/B(E2)$ ratios are much larger than those observed in Fig. 10(b). Thus, two low-lying quasineutrons are likely coupled to the $\pi h_{11/2}\nu h_{11/2}$ configuration to form band 4. The parity of this structure was suggested to be positive, therefore, using the [541]1/2 neutron with either the [411]1/2 or [402]5/2 neutrons is restricted. Instead, a calculation using the $\pi h_{11/2}\nu(h_{11/2},d_{5/2},d_{3/2}/s_{1/2})$ configuration was performed with the results shown as the dot-dashed line in Fig. 10(b). A good agreement is achieved with the experimental values, especially above spin 18, and this configuration is tentatively assigned to band 4.

TABLE IV. Parameters used in the calculation of $B(M1)/B(E2)$ values for bands in ^{128}Pr.

Configuration	g_K	i_x ($\hbar$)	K ($\hbar$)
$\pi h_{11/2}$	1.51	4.5	1.5
$\pi g_{9/2}$	1.32	0.5	4.5
$\nu h_{11/2}$	−0.32	1.5	3.5
$\nu d_{5/2}$	−0.49	0.7	2.5
$\nu d_{3/2}/s_{1/2}$	1.91	0.5	0.5
F_pG_p	1.51	4.5	0

A reasonable fit of the theoretical $B(M1)/B(E2)$ values for the $\pi g_{9/2}\nu h_{11/2}$ configuration (solid line) is seen for band 7 in Fig. 10(b). However, the experimental ratios are consistently below the calculated values. As stated previously, this configuration may be highly deformed; therefore, calculations were performed assuming band 7 has a quadrupole moment 20% larger than the normal deformed bands and the results are displayed as the dotted line in Fig. 10(b). An improved agreement with the data is seen.

Transition strength ratios for bands 5 and 6 are shown in Fig. 10(c) and excellent agreement is found for band 6 with the predicted $\pi h_{11/2}\nu d_{5/2}$ configuration (solid line) above $I=(11)$. Below this spin, band 6 mixes strongly with band 5, which has the $\pi h_{11/2}\nu(d_{3/2}/s_{1/2})$ configuration. The theoretical $B(M1)/B(E2)$ ratios for this configuration are nearly zero, as shown by the dot-dashed line in Fig. 10(c). This mixing accounts for the lower than expected ratios for band 6 and the greater than expected ratios for band 5 in the spin region below $I=(11)$.

C. Alignments and $B(M1)/B(E2)$ ratios for ^{126}Pr

In order to ascribe configurations to bands 1 and 2 in ^{126}Pr, we show the alignments of both bands in Fig. 11(a), along with the $\pi h_{11/2}$ band in ^{127}Pr [25]. It should be noted that three transitions of energies 1201, 1274, and 1351 keV were observed in the present data above the highest state in ^{127}Pr reported by Mullins *et al.* [25]. The Harris parameters of $\mathcal{J}_0=18\hbar^2/\mathrm{MeV}$ and $\mathcal{J}_1=22\hbar^4/\mathrm{MeV}^3$ were used once again. In addition, the $B(M1)/B(E2)$ ratios extracted for band 1 are displayed in Fig. 11(b).

The alignment for band 1 in ^{126}Pr is nearly identical to band 1 in ^{128}Pr [see Fig. 8(a)] below a frequency of 0.4 MeV. Similar to the $\pi h_{11/2}$ band in ^{127}Pr, band 1 in ^{126}Pr has an alignment gain above $\hbar\omega=0.4$ MeV with a large interaction strength. Two differing interpretations of this crossing have been suggested for ^{127}Pr, one being the second proton F_pG_p crossing [25], the other stating that the crossing is composed of both the EF neutron and F_pG_p proton alignments, with the EF alignment playing the dominant role [38]. As this neutron alignment has been observed above $\hbar\omega=0.6$ MeV in ^{128}Pr [see Fig. 8(c)] and in ^{129}Pr [26], it does not seem likely that the interaction near $\hbar\omega\approx0.43$ MeV would be caused by the EF crossing. Instead, we agree with Mullins *et al.* [25] that the F_pG_p alignment occurs at this frequency and with our new data, it appears that a second crossing just below $\hbar\omega=0.6$ MeV can be observed in Fig. 11(a) for ^{127}Pr. We attribute this latter alignment to the EF neutron crossing as its crossing frequency is consistent with that observed in ^{128,129}Pr.

Band 1 in ^{126}Pr undergoes the F_pG_p crossing and appears to block the EF crossing in Fig. 11(a). Only the $\pi h_{11/2}\nu h_{11/2}$ configuration can satisfy these two conditions and thus it has

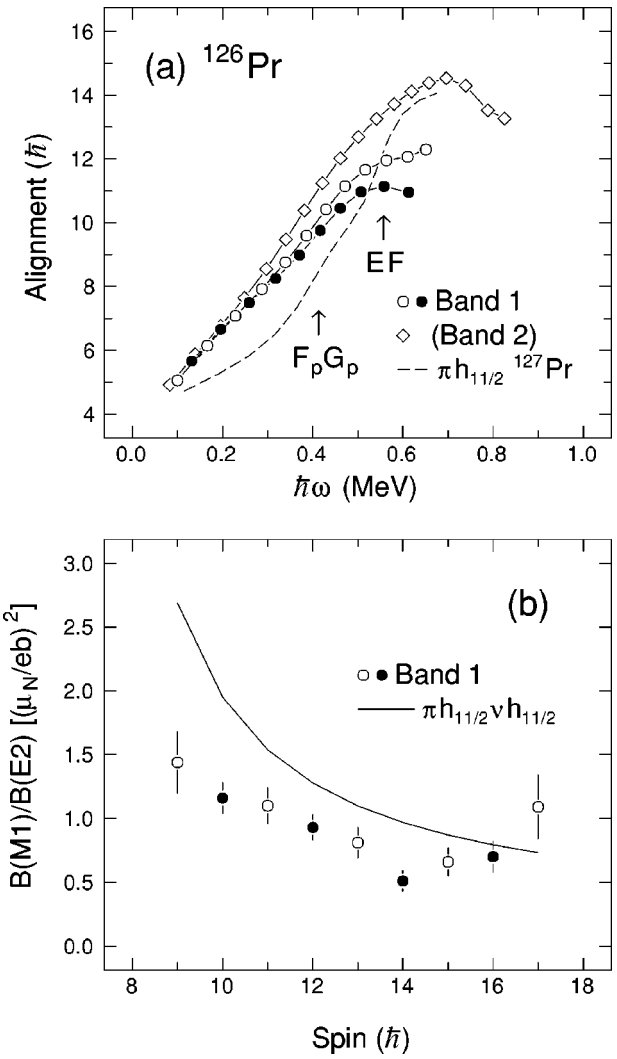

FIG. 11. (a) Alignments for the bands in ^{126}Pr where the Harris parameters of $\mathcal{J}_0 = 18\hbar^2$/MeV and $\mathcal{J}_1 = 22\hbar^4$/MeV^3 were used to subtract the angular momentum of the rotating core. The $\pi h_{11/2}$ band from ^{127}Pr is also shown for reference. Observed crossings are designated in the figure. Filled (empty) symbols denote the $\alpha = 0$ (1) sequence. (b) Extracted $B(M1)/B(E2)$ ratios for band 1 in ^{126}Pr. Filled (empty) symbols represent the experimental values for the $\alpha = 0$ (1) sequence. Calculated values (as described in the text) for the $\pi h_{11/2} \nu h_{11/2}$ configuration are shown as the solid line.

been assigned to band 1. The $B(M1)/B(E2)$ ratios for this band are compared with the predicted values of the $\pi h_{11/2} \nu h_{11/2}$ configuration in Fig. 11(b). TRS calculations suggest a deformation of $\beta_2 = 0.30$; therefore a Q_0 value of 5.1eb was used with $g_R = 0.47$ and the same g_K, i_x, and K values listed in Table IV. A reasonable agreement is found between the experimental data and theory.

As was stated previously, Petrache *et al.* [23] suggested that the spins of band 1 in ^{126}Pr should be higher by 2$\hbar$ with respect to our assignment. In the frequency range of 0.2–0.3 MeV, one may see in Fig. 11(a) that band 1 has $\sim$1.5 $\hbar$ more alignment than $\pi h_{11/2}$ in ^{127}Pr. The extra alignment is a result of the unpaired $h_{11/2}[523]7/2$ neutron and the difference is consistent with the initial alignment observed in nearby odd-N nuclei [27,39]. If the spins are increased by 2 $\hbar$, the relative alignment of band 1 is 3.5 $\hbar$ higher than the neighboring $\pi h_{11/2}$ band. The latter scenario is not consistent with the experimental data as the [523]7/2 neutron is not commonly associated with this large amount of alignment. Of course if one chooses to do the comparison at $\hbar\omega = 0.1$ MeV, then the assignment by Petrache *et al.* does make more sense. However, the high density of states at low energy and possibly strong interactions can have a large influence on the energies of the lower-spin states in bands of odd-odd nuclei. It is better, in our opinion, to do a comparison at higher frequencies, where the Coriolis force dominates and the state density decreases. We are in agreement with Petrache *et al.* that an experimental measurement of the spin would be the best solution.

The alignment of band 2 in ^{126}Pr shows a consistent gain up to $\hbar\omega \approx 0.7$ MeV [see Fig. 11(a)]. It is difficult to distinguish where the crossings take place; however, since the total alignment gain is nearly equal to that of the $\pi h_{11/2}$ band in ^{127}Pr, it is likely that the F_pG_p and EF alignments occur with very large interaction strengths. Therefore, an $h_{11/2}$ proton is most probably coupled with a low-K neutron in order to form this doubly decoupled sequence. The [541]1/2 and [411]1/2 neutrons are both good possibilities, but we favor the $\pi h_{11/2} \nu (h_{9/2}/f_{7/2})$ assignment as these bands are observed to become nearly yrast at the highest spins observed in ^{128,130,132}Pr [31]. Since band 2 is observed up to such high frequencies, it would seem likely that it also becomes yrast at very high spins. However, we cannot completely rule out the alternative configuration. As odd spins have been observed for the $\pi h_{11/2} \nu (h_{9/2}/f_{7/2})$ bands in the heavier Pr nuclei, odd spins have also been assigned for band 2. A comparison of the energy spacings of band 2 with the similar bands in ^{128,130,132}Pr has been performed in order to assign the specific spins; however, it must be stressed that these are tentative.

IV. SIGNATURE INVERSION IN THE $\pi h_{11/2} \nu h_{11/2}$ BANDS

Signature is the quantum number associated with the rotation of an axially deformed nucleus around a principal axis by 180°. The eigenvalues of the rotation operator $[\mathcal{R}_x(\pi)]$ are defined as $r = e^{i\pi\alpha}$ and one finds [33] for integer spin I that $r = (-1)^I$. Thus, $\Delta I = 2$ sequences with even (odd) spin have $r = 1 (r = -1)$, which corresponds to $\alpha = 0 (\alpha = 1)$ in the definition of the rotation operator eigenvalue noted above. It is most common to use α to denote signature due to the fact that it is an additive quantity. In a strongly coupled structure, such as band 1 in ^{126,128}Pr, both $\alpha = 0$ and 1 sequences are observed and are nearly degenerate. However, a difference in energy between the signatures, referred to as signature splitting, is expected as a result of Coriolis mixing with $K = 1/2$ orbitals, which have a decoupling parameter that pushes one signature lower in energy versus the other [33]. The signature that is lowered is dependent on the total angular momentum j of the shell from which the orbital originates. For an odd-odd nucleus, the expected energetically favored signature of a configuration is defined by $\alpha_f = |\frac{1}{2}(-1)^{j_p - 1/2} + \frac{1}{2}(-1)^{j_n - 1/2}|$, where j_p and j_n are the angular momenta of the shells associated with the valence

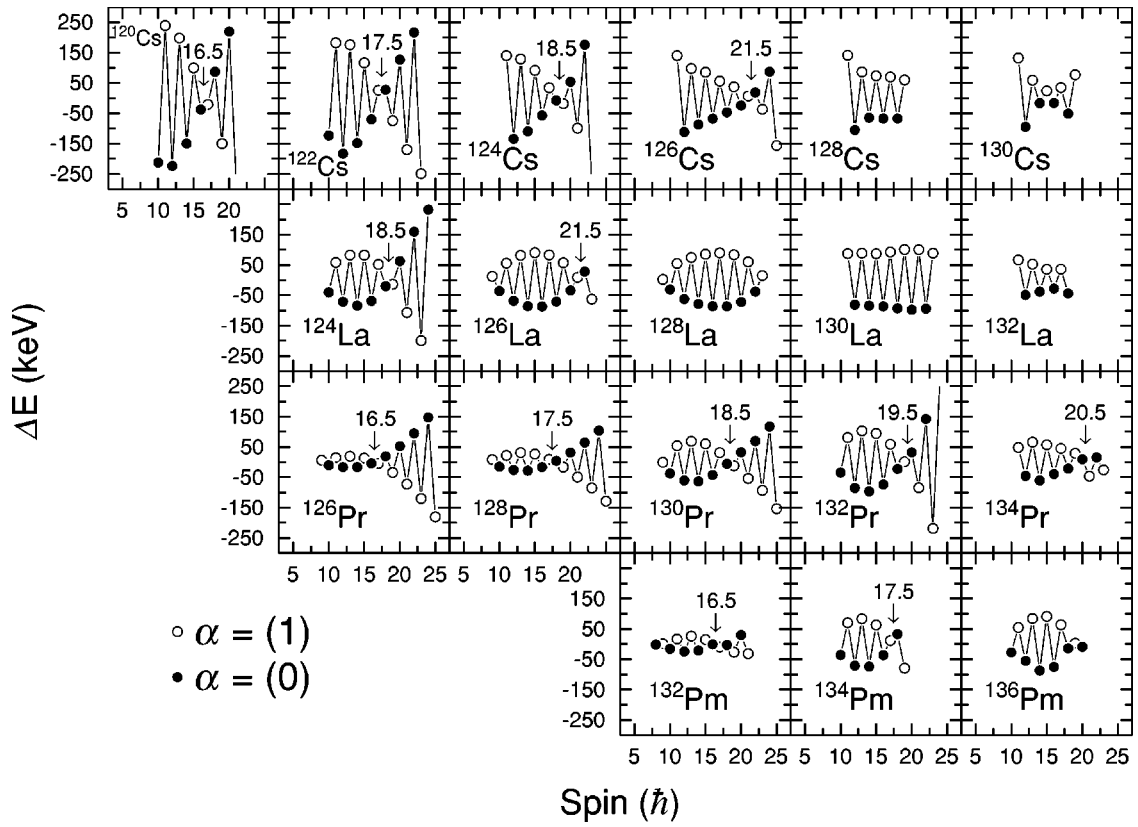

FIG. 12. Signature splitting of $\pi h_{11/2}\nu h_{11/2}$ bands in the $A\approx 130$ region. Filled (empty) symbols represent the $\alpha=0$ (1) signature. The reversion spins (as described in text) are displayed whenever possible.

nucleons. Therefore, the $\pi h_{11/2}\nu h_{11/2}$ structures (band 1 in ^{126,128}Pr) are expected to have the $\alpha=1$ signature (odd spins) favored over the $\alpha=0$ sequence.

Signature splitting may be represented in many ways, and we have chosen to use the quantity $\Delta E=[E(I)-E(I-1)]-[E(I+1)-E(I)+E(I-1)-E(I-2)]/2$ to define the energy staggering of the $\pi h_{11/2}\nu h_{11/2}$ bands shown in Fig. 12. The figure displays the splitting in this configuration for the known $65\leqslant N\leqslant 75$ Cs($Z=55$),La($Z=57$),Pr($Z=59$), and Pm ($Z=61$) nuclei. Data from nuclei not presented in this paper were compiled from the following sources: ^{120}Cs [40,41], ^{122}Cs [42], ^{124,126}Cs [43], ^{128}Cs [44], ^{130}Cs [45], ^{124}La [43], ^{126}La [46], ^{128,130}La [6], ^{132}La [8], ^{130}Pr [14], ^{132}Pr [47], ^{134}Pr [48], ^{132}Pm [49], ^{134}Pm [50], ^{136}Pm [51]. Points that have negative values are energetically favored over those with positive values. Spin values suggested by Liu *et al.* [5,52] were applied to each of the bands shown in Fig. 12. It can be seen in this figure that at lower spins, it is the $\alpha=0$ signature that is favored rather than the $\alpha=1$ sequence. Such behavior has been termed *signature inversion* [53]. As we have stated above, deducing spins for bands in odd-odd nuclei is difficult and one may wonder if the spin assignments are incorrect by one unit of $\hbar$. However, one may notice that at higher spins, normal ordering is restored. The spin at which normal ordering occurs will be defined as the ''reversion spin'' in this paper. The Coriolis force, which does not favor signature inversion, increases with frequency; therefore, it is much more likely that normal ordering will be observed at high spin versus low spin.

Comparisons of signature inversion trends in the $A\approx 130$ region are made with those found in the $A\approx 160$ region below. The smooth systematic behavior for the $A\approx 160$ nuclei is discussed in (i) below, while abnormalities in initial splitting and reversion spin are identified for the $A\approx 130$ region in (ii) and (iii), respectively. Possible explanations for the cause of inversion are also addressed in these sections.

(i) Bengtsson *et al.* [53] first introduced signature inversion in the $\pi h_{11/2}\nu i_{13/2}$ band of $^{154}_{65}$Tb$_{89}$ and suggested that it was a result of the high-j, low-K $i_{13/2}$ neutron driving the nuclear shape towards positive ($\gamma>0°$) triaxial deformation. The systematics of the $A\approx 160$ region [54,55] lend credence to this assertion. For a given isotope chain of Tb, Ho ($Z=67$), Tm ($Z=69$), or Lu ($Z=71$), the amount of initial splitting decreases as the neutron number increases from $N=89$ indicating that the force(s) causing the inversion is becoming less influential with increasing N. The nuclei become more deformed and resistant to shape polarizing effects of individual nucleons with increasing N; therefore, the $i_{13/2}$ neutron has a lessening influence on the nuclear shape. The reversion spin also decreases systematically as N increases, which also indicates that the signature inversion force(s) weakens with increasing β_2 deformation. Good systematic trends are also observed in the isotone chains as the initial splitting and reversion spin increases with Z. Within an isotone chain, the nuclei become less deformed and more susceptible to deformation driving particles as Z increases.

Although the smooth systematics in the $A\approx 160$ region do

support the idea that triaxiality plays a significant role in creating signature inversion, other theoretical studies indicate that a pn interaction [56,57] or quadrupole-quadrupole (QQ) pairing [58] can also possibly explain this phenomenon in the $\pi h_{11/2}\nu i_{13/2}$ bands. Whatever the theory chosen, it is more significant for systematic trends to be well described in a region rather than describing a few nuclei well. With this in mind and the fact that more information on odd-odd $A\approx 130$ nuclei has been published recently, we turn our attention to the $\pi h_{11/2}\nu h_{11/2}$ bands in order to illuminate their experimental trends.

(ii) Upon examining Fig. 12, one can see for a given isotone chain that the initial amount of signature splitting (between $I=10-15$) generally decreases as Z increases. The deformation increases with Z as the Fermi surface moves away from the $Z=50$ spherical shell gap, thus a similar triaxiality argument (where the high-j, low-K $h_{11/2}$ proton drives towards $\gamma>0°$) as the one asserted for the $A\approx 160$ region may seem appropriate. However, other trends do not support such an explanation for the whole region. For example, the initial splitting of the Cs nuclei decreases with N and the initial splitting of the La nuclei remains nearly constant. The heavier Cs and La nuclei are approaching the $N=82$ spherical shell gap, and thus deformation is likely decreasing with N. Applying the triaxial theory with this information, one would expect the splitting to increase with N. Indeed, this is what is observed in the Pr and Pm isotopic chains. Thus, triaxiality may describe the signature inversion in these latter nuclei, but it clearly cannot explain the trends in Cs and La on its own. Recently Xu *et al.* [58] were able to reproduce the Cs systematics without using large positive γ deformation, but included a QQ pairing term in their TRS calculations. They found that the force associated with QQ pairing inverted the signatures and decreased as N went from 65 to 71. Similar results were found for La nuclei, which did not reproduce the constant experimental trend as well, and no calculations were performed for the Pr or Pm nuclei. Particle-rotor model (PRM) calculations also indicate that a pn interaction may play a significant role in signature inversion for Cs and La [56,59].

(iii) In addition to the initial splitting, the reversion spin in the $A\approx 160$ region also varies in a systematic way. By inspecting the isotope chains in Fig. 12, one also finds gradual increases of the reversion spin as N increases for the $\pi h_{11/2}\nu h_{11/2}$ bands. This suggests that whatever is causing the inversion is able to resist the Coriolis force up to higher spins as N increases. Such a scenario is consistent with triaxiality causing the inversion as the nuclei become more prone to shape-driving nucleons with N.

The smooth trends in the reversion spin are dependent upon the spin assignments of Liu *et al.* [5,52] being correct. Recently, Lu *et al.* [60] and Gizon *et al.* [61] experimentally confirmed the suggested spin in ^{124}Cs, while Moon *et al.* [62] have determined that the the spin of the $\pi h_{11/2}\nu h_{11/2}$ band in ^{122}Cs should be increased by 2 $\hbar$ over the previous assignment. Thus, trends in the reversion spin cannot be confirmed; however, the ''reversion frequency'' is plotted in Fig. 13. The reversion frequency is defined as the frequency

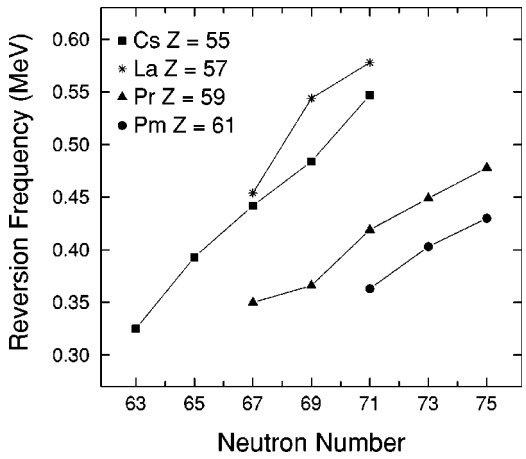

FIG. 13. Reversion frequency (as defined in the text) for the $\pi h_{11/2}\nu h_{11/2}$ bands in the $A\approx 130$ region.

where the Routhian[1] of the $\alpha=1$ sequence crosses the Routhian of the $\alpha=0$ sequence and becomes yrast. In this way, the spin dependence is essentially removed[2] from determining where the signature inversion stops.

Figure 13 shows that the reversion frequency systematically increases with N for a given isotope chain. A general trend of increasing reversion frequency with decreasing Z is also seen in the isotones. This coincides with the triaxiality argument, as the nuclei become softer as Z decreases due to the presence of the $Z=50$ spherical shell gap. However, the La nuclei surprisingly do not follow this trend as their reversion frequency is consistently higher than all the other nuclei. Indeed, one may notice the gap between the Cs ($Z=55$) and Pr ($Z=59$) nuclei in Fig. 13, where the La ($Z=57$) values might be expected to occur. Such an inconsistency cannot be explained by triaxiality alone and clearly shows the complexity of understanding signature inversion in this region.

Explaining the experimental trends in the $\pi h_{11/2}\nu h_{11/2}$ bands of the $A\approx 130$ region presents a much more difficult challenge than the $\pi h_{11/2}\nu i_{13/2}$ bands of the $A\approx 160$ region. It appears that the Pr and Pm nuclei follow similar trends to those observed in the $A\approx 160$ region and triaxiality may play a key role in describing their trends. Triaxiality cannot account for the decreasing initial splitting with N trend in Cs, but another force, such as QQ-pairing [58], must be a dominant factor. However, this force does not influence the Pr and Pm nuclei as it does Cs, so perhaps it wanes with Z. If this is the case, the La isotopes are in a transitional region where the leading factors of signature inversion in the lighter and heavier nuclei may combine and create more resistance against the Coriolis force, thus explaining the large reversion frequencies. A systematic theoretical study of these nuclei is desirable in order to better understand signature inversion in

[1]The Routhian is the energy of the quasiparticle in the rotating reference frame.

[2]The spin dependence is not completely removed as the rotational frequency is a function of I. However, changing the spin by $2\hbar$ changes the reversion frequency by less than 2%.

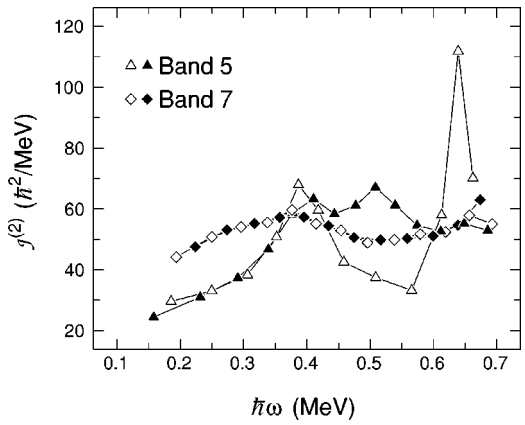

FIG. 14. The dynamical moments of inertia for bands 5 and 7 in ^{128}Pr. Filled (empty) symbols denote the $\alpha=0$ (1) signature.

this region. It would be interesting to know whether the QQ pairing has a lesser effect on the Pr and Pm nuclei, as well as an investigation into the systematic effects of the pn interaction through PRM calculations of the entire region.

V. POSSIBLE HIGHLY DEFORMED BANDS IN ^{128}Pr

The dynamical moments of inertia [$\mathcal{J}^{(2)}$] for bands 5 and 7 are plotted versus rotational frequency in Fig. 14. At a frequency of 0.25 MeV, band 5 is found to have $\mathcal{J}^{(2)} \approx 30\hbar^2$/MeV, which is a typical value for most bands in ^{128}Pr. Band 7, whose configuration is $\pi g_{9/2}\nu h_{11/2}$, has $\mathcal{J}^{(2)} \approx 50\ \hbar^2$/MeV at this same frequency. A large dynamical moment of inertia is often associated with a larger deformation. Indeed, a band with the same configuration in ^{130}Pr is found to have a similar increase in $\mathcal{J}^{(2)}$ over the normal deformed structures, and a quadrupole moment of $Q_0 = 6.1(4)e$b was measured for the $\pi g_{9/2}\nu h_{11/2}$ sequence [63]. This establishes the highly deformed character of this configuration as a quadrupole moment of $Q_0 = 3.4(2)e$b was determined for the normal deformed bands in the same experiment. In addition, Smith *et al.* [14] reported that extended TRS calculations predict a deformation of $\beta_2 = 0.337$ for band 7 in ^{128}Pr, while $\beta_2 = 0.291$ is expected for the $\pi h_{11/2}\nu h_{11/2}$ configuration.

Referring to Fig. 8(c), one observes that the $\alpha=1$ signature of band 5[$\pi h_{11/2}\nu(d_{3/2}/s_{1/2})$] has an alignment gain after the F_pG_p crossing, but well before the observed EF crossing in its signature partner. By inspection of Fig. 14, the $\mathcal{J}^{(2)}$ of the $\alpha=1$ signature in band 5 also remains high at $\sim 60\hbar^2$/MeV after the crossing at 0.51 MeV. In fact this is near the same value as observed for the $\pi g_{9/2}\nu h_{11/2}$ band, indicating that this sequence may be highly deformed at the highest frequencies. The quasineutron Routhians in Fig. 9(b) show that the intruder $i_{13/2}$ neutron is predicted to interact with the $d_{3/2}/s_{1/2}$ [411]1/2 neutron near 0.5 MeV, and is in excellent agreement with the observed crossing frequency of $\sim$0.51 MeV. Thus, we suggest the $i_{13/2}$[660]1/2 neutron, which is known to drive the nuclear shape to higher deformations [64], adiabatically crosses with the $\pi h_{11/2}\nu(d_{3/2}/s_{1/2})$ normal deformed configuration.

The $i_{13/2}$ neutron is also found to adiabatically cross bands in other well-deformed, odd-N nuclei in the mass 130 region, such as $^{135}_{62}\mathrm{Sm}_{73}$ [65] (at $\hbar\omega \approx 0.3$ MeV), $^{131}_{60}\mathrm{Nd}_{71}$ [66] (at $\sim$0.34 MeV), and $^{129}\mathrm{Nd}_{69}$ [27] (at $\sim$0.45 MeV). A trend is observed where the crossing frequency increases with decreasing N. This is understandable as the $\nu i_{13/2}$ orbital is located higher above the Fermi surface as N decreases. In addition, the crossing frequency increases in the $N=69$ nuclei from ^{129}Nd($\sim$0.45 MeV) to ^{128}Pr($\sim$0.51 MeV). A decrease in the ground-state deformation from $Z=60$ to 59 likely causes the Fermi surface in ^{128}Pr to be further away from the [660]1/2 orbital than in ^{129}Nd.

VI. SUMMARY

A significant extension of the ^{128}Pr level scheme and the first identification of excited states in ^{126}Pr was made possible through the use of large Ge arrays (Gammasphere and Clarion), light charged particle arrays (Microball and Hy-Ball), and a recoil mass spectrometer (RMS). Configuration assignments were made for each of the structures based on observed rotational alignments, $B(M1)/B(E2)$ ratios, and signature splitting. The discrepancy in the interpretation of the first crossing (at $\hbar\omega \approx 0.4$ MeV) observed in the $\pi h_{11/2}$ band of ^{127}Pr is resolved as the second proton crossing is observed near this frequency in ^{128}Pr, while the first neutron alignment is not observed until $\sim$0.6 MeV. Experimental trends in the signature inversion of $\pi h_{11/2}\nu h_{11/2}$ bands were discussed in detail. Although very regular systematics appear in the signature inversion of $\pi h_{11/2}\nu i_{13/2}$ bands in the $A \approx 160$ region, several irregularities occur in the $A \approx 130$ nuclei. Most notably, the reversion frequencies of the La nuclei are surprisingly large with respect to the other nuclei. The highly deformed $\pi g_{9/2}\nu h_{11/2}$ configuration was observed to be based upon an isomeric state with a half-life greater than 80 ns. Evidence for the intruder $i_{13/2}$ neutron adiabatically crossing with one of the normal deformed sequences was also observed.

ACKNOWLEDGMENTS

The authors wish to thank the ANL and ORNL operations staffs for their valuable help. Special thanks to J. Greene for target preparation and to H. Q. Jin for his software support. This work was funded by the U.S. Department of Energy through Contract Nos. DE-FG02-96ER40983 (University of Tennessee), W-31-109-ENG-38 (Argonne National Laboratory), and DE-FG05-88ER40406 (Washington University). ORNL is managed by UT-Battelle for the U.S. DOE under Contract No. DE-FG02-96ER49083.

[1] F.G. Kondev, G.D. Dracoulis, A.P. Byrne, and T. Kibédi, Nucl. Phys. **A632**, 473 (1998).
[2] D.M. Cullen, C.-H. Yu, D. Cline, M. Simon, D.C. Radford, M.A. Riley, and J. Simpson, Phys. Rev. C **57**, 2170 (1998).
[3] W. Reviol *et al.*, Phys. Rev. C **59**, 1351 (1999).
[4] G. Levinton *et al.*, Phys. Rev. C **60**, 044309 (1999).
[5] Y. Liu, J. Lu, Y. Ma, S. Zhou, and H. Zheng, Phys. Rev. C **54**, 719 (1996).
[6] M.J. Godfrey, Y. He, I. Jenkins, A. Kirwan, P.J. Nolan, D.J. Thornley, S.M. Mullins, R. Wadsworth, and R.A. Wyss, J. Phys. G **15**, 671 (1989).
[7] J. Pfohl *et al.*, Phys. Rev. C **62**, 031304(R) (2000).
[8] K. Starosta *et al.*, Phys. Rev. Lett. **86**, 971 (2001).
[9] D.G. Sarantites, P.-F. Hua, M. Devlin, L.G. Sobotka, J. Elson, J.T. Hood, D.R. LaFosse, J.E. Sarantites, and M.R. Maier, Nucl. Instrum. Methods Phys. Res. A **381**, 418 (1996).
[10] A. Galindo-Uribarri, HyBall charged particle detector system, URL:http://www.phy.ornl.gov/hribf/research/equipment/hyball
[11] C.J. Gross *et al.*, Nucl. Instrum. Methods Phys. Res. A **450**, 12 (2000).
[12] D.J. Hartley *et al.*, Phys. Rev. C **63**, 041301(R) (2001).
[13] D. Vretenar, G.A. Lalazissis, and P. Ring, Phys. Rev. Lett. **82**, 4595 (1999).
[14] B.H. Smith *et al.*, Phys. Lett. B **443**, 89 (1998).
[15] T.M. Cormier, P.M. Stwertka, H. Herman, and N.G. Nicolis, Phys. Rev. C **30**, 195 (1984).
[16] D.C. Radford, Nucl. Instrum. Methods Phys. Res. A **361**, 297 (1995).
[17] R.V.F. Janssens and F. Stephens, Nucl. Phys. News **6**, 9 (1996).
[18] A. Krämer-Flecken, T. Morek, R.M. Lieder, W. Gast, G. Hebbinghaus, H.M. Jäger, and W. Urban, Nucl. Instrum. Methods Phys. Res. A **275**, 333 (1989).
[19] W. Reisdorf, Z. Phys. A **300**, 227 (1981).
[20] D.C.B. Watson *et al.*, Daresbury Laboratory, Annual Report No. 186-87, 1987 (unpublished), Appendix p. 31.
[21] Y. Xie *et al.*, Eur. Phys. J. A **5**, 341 (1999).
[22] T. Morek *et al.*, Eur. Phys. J. A **3**, 99 (1998).
[23] C.M. Petrache *et al.*, Phys. Rev. C **64,** 044303 (2001).
[24] A. Wilson (private communication).
[25] S.M. Mullins *et al.*, Phys. Rev. C **58**, R2626 (1998).
[26] A. Galindo-Uribarri *et al.* (unpublished).
[27] O. Zeidan *et al.*, Phys. Rev. C **65,** 024303 (2002).
[28] R. Bengtsson and S. Frauendorf, Nucl. Phys. **A314**, 27 (1979); **A327**, 139 (1979).
[29] C.J. Gallagher and S.A. Moszkowski, Phys. Rev. **111**, 1282 (1958).
[30] E.S. Paul *et al.*, Nucl. Phys. **A636**, 32 (2000).
[31] F.G. Kondev *et al.*, Phys. Rev. C **59**, 3076 (1999).
[32] A. Galindo-Uribarri *et al.*, Phys. Rev. C **50**, R2655 (1994).
[33] A. Bohr and B. Mottelson, *Nuclear Structure* (Benjamin, New York, 1975), Vol. 2.
[34] V.P. Janzen *et al.*, Phys. Rev. C **45**, 613 (1992).
[35] F. Dönau, Nucl. Phys. **A471**, 469 (1987).
[36] S. Frauendorf, Phys. Lett. **100B**, 219 (1981).
[37] S. Ćwiok, J. Dudek, W. Nazarewicz, J. Skalski, and T. Werner, Comput. Phys. Commun. **46**, 379 (1987); J. Dudek, A. Majhofer, J. Skalski, T. Werner, S. Ćwiok, and W. Nazarewicz, J. Phys. G **5**, 1359 (1979).
[38] C.M. Parry *et al.*, Phys. Rev. C **57**, 2215 (1998).
[39] E.S. Paul *et al.*, Phys. Rev. C **58**, 801 (1998).
[40] F. Liden *et al.* (private communication).
[41] C.-B. Moon, S. J. Chae, J. H. Ha, T. Komatsubara, Y. Sasaki, T. Jumastsu, K. Yamada, K. Satou, and K. Furuho, Nucl. Phys. (to be published).
[42] J.F. Smith, C.J. Chiara, D.B. Fossan, G.J. Lane, J.F. Lewicki, J.M. Sears, and P. Vaska, Phys. Rev. C **58**, 3237 (1998).
[43] T. Komatsubara *et al.*, Nucl. Phys. **A557**, 419c (1993).
[44] E.S. Paul, D.B. Fossan, Y. Liang, R. Ma, and N. Xu, Phys. Rev. C **40**, 619 (1989).
[45] R. Kumar, D. Mehta, N. Singh, H. Kaur, A. Görgen, S. Chmel, R.P. Singh, and S. Murlithar, Eur. Phys. J. A **11**, 5 (2001).
[46] B.M. Nyakó, J. Gizon, D. Barnéoud, A. Gizon, M. Józsa, W. Klamra, F.A. Beck, and J.C. Merdinger, Z. Phys. A **332**, 235 (1989).
[47] C.M. Petrache *et al.*, Nucl. Phys. **A635**, 361 (1998).
[48] K. Hauschild *et al.*, Phys. Rev. C **50**, 707 (1994).
[49] R. Wadsworth *et al.*, Daresbury Annual Report 1990–1991, Appendix, p. 13.
[50] R. Wadsworth, S.M. Mullins, P.J. Bishop, A. Kirwan, M.J. Godfrey, P.J. Nolan, and P.H. Regan, Nucl. Phys. **A526**, 188 (1991).
[51] D.J. Hartley *et al.*, Phys. Rev. C **64**, 031304(R) (2001).
[52] Y. Liu, J. Lu, Y. Ma, G. Zhao, H. Zheng, and S. Zhou, Phys. Rev. C **58**, 1849 (1998).
[53] R. Bengtsson, H. Frisk, F.R. May, and J.A. Pinston, Nucl. Phys. **A415**, 189 (1984).
[54] C.-H. Yu *et al.*, in *Proceedings of the Workshop on Gammasphere Physics*, edited by M. A. Deleplanque, I. Y. Lee, and A. O. Macchiavelli (World Scientific, Singapore, 1996), p. 254.
[55] L.L. Riedinger *et al.*, Acta Phys. Pol. B **32,** 2613 (2001).
[56] B. Cederwall *et al.*, Nucl. Phys. **A542**, 454 (1992).
[57] R. Zhang, S. Zhu, N. Cheng, and J. Wen, Phys. Rev. C **64**, 014313 (2001).
[58] F.R. Xu, W. Satula, and R. Wyss, Nucl. Phys. **A669**, 119 (2000).
[59] N. Tajima, Nucl. Phys. **A572**, 365 (1994).
[60] J. Lu *et al.*, Phys. Rev. C **62**, 057304 (2000).
[61] A. Gizon *et al.*, Nucl. Phys. **A694**, 63 (2001).
[62] C.-B. Moon, T. Komatsubara, and K. Furuno, Nucl. Phys. **A674**, 343 (2000).
[63] F.G. Kondev *et al.*, Eur. Phys. J. A **2**, 249 (1998).
[64] F.G. Kondev *et al.*, Phys. Rev. C **60**, 011303(R) (1999).
[65] S.M. Mullins, R. Wadsworth, J.M. O'Donnell, P.J. Nolan, A.J. Kirwan, P.J. Bishop, M.J. Godfrey, and D.J.G. Love, J. Phys. G **13**, L201 (1987).
[66] D.J. Hartley *et al.*, Phys. Rev. C **60**, 041301(R) (1999).